Central nervous system infiltrated immune cells induce calcium increase in astrocytes via astroglial purinergic signaling

Dunja D. Bijelić[1,#], Katarina D. Milićević[1,#], Milica N. Lazarević[2], Djordje M. Miljković[2], Jelena J. Bogdanović Pristov[3], Danijela Z. Savić[4], Branka B. Petković[5], Pavle R. Andjus[1,], Miljana B. Momčilović[2], Ljiljana M. Nikolić[5,*]

[1]Center for Laser Microscopy, University of Belgrade, Faculty of Biology, 11158 Belgrade, Serbia

[2]Department of Immunology, University of Belgrade, Institute for Biological Research *Siniša Stanković,* National Institute of Republic of Serbia, 11060 Belgrade, Serbia

[3]Department of Life Sciences, University of Belgrade, Institute for Multidisciplinary Research, 11030 Belgrade, Serbia

[4]Department of Neurobiology, University of Belgrade, Institute for Biological Research *Siniša Stanković,* National Institute of Republic of Serbia, 11060 Belgrade, Serbia

[5]Department of Neurophysiology, University of Belgrade, Institute for Biological Research *Siniša Stanković,* National Institute of Republic of Serbia, 11060 Belgrade, Serbia

[#] Dunja D. Bijelić and Katarina D. Milićević should be considered joint first author.

Abbreviated title: Astrocyte-autoreactive immune cell interaction

Keywords: astrocytes, calcium signaling, cell communication, nervous system autoimmune disease, purinergic receptors

RRID: RRID:RGD_21409748, RRID: RGD_21409752, RRID:AB_2538778, RRID:AB_10050580, RRID:AB_2629482, RRID:AB_2224402, RRID:AB_10013382, RRID:AB_10682518, RRID:AB_162543, RRID:AB_2534102, RRID:AB_162542, RRID:SCR_002285, RRID:SCR_011323, RRID:AB_1018856, RRID:AB_2828023, RRID:AB_10013382, RRID:AB_2534013, RRID:AB_2535792, RRID:SCR_003210, RRID:SCR_002798, RRID:SCR_014235

*Corresponding author: Ljiljana M. Nikolić
Department of Neurophysiology, University of Belgrade, Institute for Biological Research *Siniša Stanković,* National Institute of Republic of Serbia, 11060 Belgrade, Serbia
Despota Stefana Boulevard 142
Tel: +381 11 2078 308, +381 63 8691 484
ljnikolic@ibiss.bg.ac.rs, nikolic13@gmail.com

Funding information
This work was supported by the Ministry of Education, Science and Technological Development of Republic of Serbia (Contract no. 451-03-68/2020-14/200007, 451-03-68/2020-14/200178, 451-03-68/2020-14/200053), and a Fellowship *Start up for Science* from the Centre for Leadership Development to Ljiljana M. Nikolić.

Abstract

Interaction between autoreactive immune cells and astroglia is an important part of the pathologic processes that fuel neurodegeneration in multiple sclerosis. In this inflammatory disease, immune cells enter into the central nervous system (CNS) and they spread through CNS parenchyma, but the impact of these autoreactive immune cells on the activity pattern of astrocytes has not been defined. By exploiting naïve astrocytes in culture and CNS infiltrated immune cells (CNS IIC) isolated from rat with experimental autoimmune encephalomyelitis (EAE), here we demonstrate previously unrecognized properties of immune cell-astrocyte interaction. We show that CNS IIC but not the peripheral immune cell application, evokes a rapid and vigorous intracellular Ca^{2+} increase in astrocytes by promoting glial release of ATP. ATP propagated Ca^{2+} elevation through glial purinergic P2X7 receptor activation by the hemichannel-dependent nucleotide release mechanism. Astrocyte Ca^{2+} increase is specifically triggered by the autoreactive $CD4^{+}$ T cell application and these two cell types exhibit close spatial interaction in EAE. Therefore, Ca^{2+} signals may mediate a rapid astroglial response to the autoreactive immune cells in their local environment. This property of immune cell-astrocyte interaction may be important to consider in studies interrogating CNS autoimmune disease.

Significance statement

In multiple sclerosis and experimental autoimmune encephalomyelitis, autoreactive immune cells infiltrate into the central nervous system (CNS) that is contiguously tiled by the glial cells astrocytes. However, astroglial pattern of activity in the presence of autoreactive immune cells in their local environment has not been determined. We show that astrocytes within seconds robustly elevate their intracellular Ca^{2+} when they encounter CNS-infiltrated immune cells in their close proximity. This Ca^{2+} elevation is under the control of glial ATP-mediated signaling. Thus, astrocytes may respond rapidly to the nearby autoreactive immune cells, and this could contribute to neuropathology of CNS autoimmune disease.

Introduction

In the inflammatory demyelinating disease multiple sclerosis (MS), interactions between autoreactive immune cells infiltrating the brain and spinal cord and glial cells resident in the central nervous system (CNS), create an inflammatory environment that drives disease processes causing neurodegeneration (Mayo et al., 2012; Dendrou et al., 2015; Baecher-Allan et al., 2018). Astrocytes are an important component of this neuropathologic process. These glial cells have been shown to respond to the inflammatory mediators released by the immune cells, and in turn to produce pro-inflammatory molecules for feedback signaling to the immune cells (Rothhammer and Quintana, 2015; Colombo and Farina, 2016; Brambilla, 2019). These complex dependencies are coupled to the cellular hypertrophy and enhanced proliferation of astrocytes in the pathological sequelae of MS (Brambilla, 2019; Yi et al., 2019). In disease, autoreactive immune cells spread through CNS parenchyma, and they embed into the astroglial network that almost completely covers the CNS (Voskuhl et al., 2009). However, we know little about the activity pattern of astrocytes in the presence of immune cells in their local environment, information that is important to further our understanding of the pathologic processes in an autoimmune disease.

Because of their wide distribution and their dense meshwork in the CNS, astrocytes are ideally suited to receive and integrate numerous signals in their local environment and respond to them by releasing transmitters such as ATP and glutamate, to signal to each other and to neighboring cells in the CNS (Haydon, 2001; Parpura et al., 2012; Araque et al., 2014). Astrocytes express a wide range of receptors for transmitters and ion channels that upon activation cause transient increase in their intracellular Ca^{2+} concentration either by regulating Ca^{2+} entry into the cell or its liberation from intracellular stores (Fumagalli et al., 2003; Hamilton et al., 2008; Panatier et al., 2011; Shigetomi et al., 2013). This generates Ca^{2+} responses on a time scale of seconds and enables these glial cells to rapidly interact with neighboring cells in the CNS in physiological and pathological states (Bazargani and Attwell, 2016; Verkhratsky et al., 2019), indicating that Ca^{2+} signaling represents a fundamental property of astrocyte physiology. Nevertheless, Ca^{2+} dynamics of astrocytes and the role of Ca^{2+} signals in mediating interaction between astrocytes and autoreactive immune cells infiltrated into the CNS have not been determined.

Here, we exploited in vitro system and performed Ca^{2+} imaging to selectively define activity pattern of cultured naïve astrocytes upon application of the CNS infiltrated immune cells (CNS IIC) isolated from the spinal cord of rat with experimental autoimmune enchephalomyelitis (EAE), a commonly used animal model of MS. Our results reveal previously unrecognized CNS-immune system interaction, and demonstrate that CNS IIC can trigger a rapid Ca^{2+} increase in astrocytes through a mechanism involving astroglial purinergic signaling.

Materials and Methods

Experimental subject details

Dark Agouti rat strain was used in all experiments. Animals were housed under standard laboratory conditions in a 12 h light/dark cycle at 22-24 ºC in regularly cleaned cages, and food and water was provided ad libitum. All animals were healthy with no obvious behavioral phenotype prior to EAE induction. EAE was induced in 2-3 months old rats of both sexes (weight: ~150 g for females and ~200 g for males, RRID:RGD_21409748). Females and males were kept in separate cages, 4 animals per cage maximum. Totally 12 females and 13 males were used in experiments: 8 females and 6 males for Ca^{2+} imaging experiments; 4 females and 4 males for ATP measurement experiments; 3 males for immunohistochemistry. Dark Agouti 1-3 days old pups (~1-3 g weight, RRID: RGD_21409752), were used to prepare cultures of the spinal cord astrocytes (Naïve astrocytes, i.e. astrocytes from a healthy animal), totally 20 pups were used for experiments (2-3 pups per culture preparation). CNS IIC isolated from females and males were examined for sex-specific effects on astrocyte Ca^{2+} level. Animals were randomly allocated to Ca^{2+} imaging, ATP measurement and immunohistochemistry experiments. Experiments were conducted and analyzed blind when possible (i.e. Ca^{2+} imaging data were analyzed in a blind manner; ATP measurements were conducted and analyzed in a blind manner; immunohistochemistry staining was analyzed in a blind manner for GFAP signal). No animals were excluded from analysis. Animal procedures were carried out in accordance with the strict protocols of the Ethical Committee for the Use of Laboratory Animals of the Institute of Biological Research *Siniša Stanković* and Faculty of Biology, University of Belgrade, Serbia and in the compliance with the EU Directive (2010/63/EU) on the protection of animals used for scientific purposes.

Induction of EAE

EAE was induced in Dark Agouti strain (Miljković et al., 2011b) with rat spinal cord homogenate (SCH) in phosphate buffer saline (PBS, 50% w/v) mixed with an equal volume of complete Freund's adjuvant (CFA, Difco Detroit, MI, USA) supplemented with up to 5 mg/ml of M. tuberculosis H37Ra (Difco). Animals were injected intradermally in the hind footpad with 100 µl of SCH + CFA as previously described (Miljkovic et al., 2006). Animals were monitored daily for EAE signs, and disease score was estimated according to the following scale: no clinical signs -score 0, flaccid tail -score 1; hind limb paresis -score 2; severe hind limb paralysis -score 3. Animals were sacrificed at the late onset (10-12 days post immunization; EAE score 1) or at the peak of EAE (13-15 days post immunization, EAE scores 2 and 3).

Immune cell isolation

CNS IIC were isolated from the spinal cords of EAE rats transcardially perfused with cold sterile PBS. Each spinal cord was first homogenized by passing the tissue through the 40 µm stainless steel mesh in 5 ml of PBS supplemented with 3% of fetal calf serum (FCS) (PAA Laboratories, Pasching, Austria). Next, homogenate was centrifuged (100 × g, 10 min, at +4 ºC) and the pellet was resuspended in 3 ml of 30% Percoll (Sigma-Aldrich, Sigma-Aldrich, St. Louis, MO, USA) and overlaid on 3 ml of 70% Percoll gradient. Following centrifugation at 850 × g for 40 min, the CNS IIC were recovered from the 30%/70% Percoll interface and washed in RPMI-1640 medium (Sigma-Aldrich) supplemented with 5% FCS. Peripheral lymph node immune cells (Peripheral IC) were isolated by mechanical disruption of the cervical lymph nodes through a 40 µm stainless steel mesh in 5 ml of PBS supplemented with 3% FCS. CNS IIC and Peripheral IC were isolated from the same animals throughout experiments. As previously described, CNS IIC isolate contains predominantly T cells, and in lower percentages macrophages, monocytes, granulocytes and NK cells (Miljković et al., 2011a). To further purify infiltrated $CD4^+$ T cells ($CD4^+$ CNS ITC) from this CNS IIC population we used biotin conjugated antibody specific for CD4 (Thermo Fisher Scientific, Cat# MA5-17388, RRID:AB_2538778) and IMag SAv particles plus (BD Biosciences, Cat# 557812, RRID:AB_10050580). Quantification and purity of the $CD4^+$ CNS ITC was determined by the flow cytofluorometry analysis on a CyFlow Space flow cytometer (Partec, Munster, Germany). There was > 95% of $CD4^+$ T cells in the purified CNS IIC population. After $CD4^+$ CNS ITC purification, the rest of the CNS IIC population was

collected (CNS IIC without $CD4^+$ ITC). All isolated immune cells were kept in the RPMI-1640 medium on ice and maintained under the same conditions until further use.

Spinal cord astrocyte culture preparation

After isolation of the spinal cord, meninges were carefully removed and the tissue was mechanically dissociated under sterile conditions in the ice-cold Dulbecco's modified Eagle medium-low glucose (DMEM, Sigma-Aldrich). After two centrifugation washing steps at 500 × g for 4 min, cells were passed through sterile 21G and 23G needles 3-5 times, followed by centrifugation washing step at 500 × g for 4 min. Cells were resuspended in DMEM supplemented with 10% fetal bovine serum (Gibco, Thermo Fisher Scintific, MA, USA), D-glucose in final concentration of 25 mM/l (Sigma-Aldrich), 100 IU/ml penicillin and 100µg/ml streptomycin (Gibco), afterwards seeded (2 to 3 spinal cords per culture preparation) in a 60 mm Petri dish and grown in a humidified atmosphere of 5% CO_2/95% air at 37 °C. Culture medium was replaced every 2-3 days until cells reached 80% confluence (after 7 to 10 days in vitro). Cell culture was then washed with DMEM medium using pipette to mechanically remove loosely attached glial cells. Underlying layer of astrocytes was trypsinized (0.25 % trypsin and 0.02 % EDTA, Sigma-Aldrich) and plated in a Petri dish at a low 10^4 cells/cm^2 density. Next, after reaching 50% confluence, during each medium replacement cell culture was repeatedly washed with DMEM to minimize contamination of astroglial layer with other types of glia. Upon reaching 80% confluence (after 14 to 20 days in vitro), astrocytes were collected after trypsinization, and seeded on 7 mm circular glass coverslips (MenzelGlasser, Braunschweig, Germany) coated with poly-L-lysine (50 µg/ml, Sigma-Aldrich) at the density of 5×10^3 cells per coverslip, and used for imaging 48 to 72 h later.

Assessment of culture purity

Applied culturing procedure yielded cells that had typical morphology of astrocytes. Rarely, we observed few microglial cells that were clearly morphologically different from astrocytes, and were not included in analysis. To assess the culture purity, routine immunostaining was performed. Coverslips with seeded cells were rinsed in PBS, fixed in 4% paraformaldehyde (PFA, Sigma-Aldrich) for 20 min, and rinsed in PBS again. Then to prevent binding of antibodies to non-specific epitopes, coverslips were incubated for 60 min at room temperature in a blocking buffer (0.1% Triton X-100, 10% normal donkey serum and 10% bovine serum

albumin (Sigma-Aldrich) in PBS)). For immunolabeling, coverslips were incubated with primary antibodies diluted in blocking buffer overnight at 4 ºC. After rinsing with PBS, coverslips were incubated with fluorescent dye-conjugated secondary antibodies diluted in blocking buffer for 2.5 h in dark at room temperature. Following rinsing in PBS, cells were incubated with a nuclear counterstain 4',6-Diamidino-2-Phenylindole, Dihydrochloride (DAPI; 1:4000, Thermo Fisher Scientific, Cat# D1306, RRID:AB_2629482) or Hoest 33342 (1 µg/ml, Thermo Fisher Scientific, Cat# H3570) for 10 min, rinsed in PBS, and mounted with Mowiol (Sigma-Aldrich). Primary antibody used: rabbit anti-GFAP (1:300, Agilent, Cat# Z0334, RRID:AB_10013382), goat anti-Iba1 (1:200, Abcam, Cat# ab5076, RRID:AB_2224402), mouse anti-CNPase (1:200, Millipore, Cat# NE1020-100UL, RRID:AB_10682518). Secondary antibodies used (raised in donkey): Alexa Fluor 555- (1:200, Thermo Fisher Scientific Cat# A-31572, RRID:AB_162543), Alexa Fluor 488- (1:200, Molecular Probes, Cat# A-11055, RRID:AB_2534102), Alexa Fluor 647- (1:200, Molecular Probes, Cat# A-31571, RRID:AB_162542) conjugated secondary antibodies to rabbit, goat or mouse. Images were acquired on a confocal laser scanning microscope (LSM 510, Carl Zeiss GmbH, Jena, Germany) using 40X DIC oil objective and monochrome camera AxioCam ICm1 (Carl Zeiss, GmbH, Germany) and inverted epifluorescent microscope AxioObserver A1 (Carl Zeiss, Oberkochen, Germany). Cells were analyzed using Fiji ImageJ software (www.fiji.sc, RRID:SCR_002285). The presence of $GFAP^+$, $Iba1^+$, and $CNPase^+$ cells was determined relative to the total number of nuclei (DAPI staining) in the field of view.

Time-lapse Fluorescence Imaging

Fluorescence changes arising from Fluo-4 AM (Molecular Probes, Eugene, OR, USA) were recorded from individual spinal cord astrocytes in culture. Astrocytes were loaded with the Ca^{2+} indicator Fluo-4 AM (5 µM) at room temperature for 30 min in extracellular solution (ECS) containing (in mM): 140 NaCl, 5 KCl, 2 $CaCl_2$, 2 $MgCl_2$, 10 D-glucose (all from Sigma-Aldrich), and 10 HEPES (Biowest, Nuaillé, France), pH 7.4, 300 mOsm. After rinsing, cells were kept in ECS for 15-30 min to allow Fluo-4 AM de-esterification. Time-lapse Ca^{2+} imaging was carried out by using a AxioObserver A1 microscope with a LD LCI Plan-Apochromat 25X/0.8NA water immersion objective lens (Carl Zeiss), a ”evolve”-EM 512 Digital Camera System (Photometrics, Tucson, AZ, USA), and VisiView® high performance software (VisiChrome, Visitron Systems GmbH, Puchheim, Germany). Fluo-4 fluorophore was excited at

480 nm using Xenon Short Arc lamp (Ushio, Japan) coupled to the VisiChrome Polychromatic Illumination System (Visitron Systems). Excitation and the emission light passed through the FITC filter set (Chroma Technology Inc., VT, USA). Frame scanning mode was performed at a frequency of 1 Hz. During experiments astrocytes were perfused with ECS at perfusion speed of 4 ml/min. Isolated immune cells were first centrifuged at 500 × g, then resuspended in ECS and maintained at +4 ºC. Immune cells were placed for at least 15 min at room temperature before further use. Isolated immune cells were bath applied for 20-30 s in the close vicinity of astrocytes using custom made perfusion system. Application system was positioned at the edge of the field of view, 1 mm above the coverslip surface and at the angle of 45º. To confirm that applied isolated immune cells reached astrocytes with this application system, in a subset of experiments we loaded only CNS IIC with Fluo-4 AM for purpose of visualization. The procedure for labeling CNS IIC with Fluo-4 AM was the same as for astrocytes, except that before the incubation step with Fluo-4AM and rinsing step, CNS IIC were first centrifuged at 500 × g.

CNS IIC were applied at concentrations of 5×10^3, 25×10^3 and 50×10^3 cells/ml, in the range of infiltrating immune cell concentrations measured in the spinal cord parenchyma of EAE rat (Schläger et al., 2016). Experiments using different CNS IIC concentrations were randomly interleaved. Peripheral IC were applied at the 25×10^3 cells/ml concentration. In a subset of experiments astrocytes were imaged upon application of CNS IIC or their ECS that has been conditioned by soluble factors released by the immune cells within 1-4 h (CNS IIC-conditioned medium). To obtain CNS IIC-conditioned medium we removed CNS IIC by centrifugation at 500 × g and collected their ECS. Experiments with CNS IIC or their matched conditioned medium were randomly interleaved. Experiments with $CD4^+$ CNS ITC and CNS IIC without $CD4^+$ ITC were randomly interleaved with the total CNS IIC population from which they were purified (each applied at the concentration of 25×10^3 cells/ml). In experiments using inhibitors of astrocyte receptors, astrocytes were first incubated for 10 min in each drug to produce an effective receptor block, and then the drugs were bath applied during the course of experiments. In a set of experiments when we interrupted vesicular ATP release, astrocytes were preincubated in brefeldin A (2 μg/ml, Sigma-Aldrich), an inhibitor of vesicular trafficking for 60 min (Bowser and Khakh, 2007). Data in the presence of the drugs were compared with randomly interleaved

control data obtained without the drugs. ATP (200 μM, Sigma-Aldrich) was applied at the end of each experiment to check the viability of astrocytes.

The following drugs were used in experiments: MPEP (2-Methyl-6-(phenylethynyl)pyridine hydrochloride) to block mGluR5, MRS2179 (2'-Deoxy-N6-methyladenosine 3',5'-bisphosphate tetrasodium salt) to block P2Y1 receptors and A967079 (1E,3E)-1-(4-Fluorophenyl)-2-methyl-1-pentene-3-one oxime) to block TRPA1 channels (all from Abcam, Cambridge, UK); CPCCOEt (7-(Hydroxyimino)cyclopropa[b]chromen-1a-carboxylate ethyl ester) to block mGluR1, PPADS (Pyridoxalphosphate-6-azophenyl-2',4'-disulfonic acid tetrasodium salt) to block P2, A438079 (3-[[5-(2,3-Dichlorophenyl)-1H-tetrazol-1-yl]methyl]pyridine hydrochloride) to block P2X7, BzATP (2'(3')-O-(4-Benzoylbenzoyl)adenosine-5'-triphosphate tri(triethylammonium) salt) to activate P2X7 receptors (all from Tocris Bioscience, Bristol, UK); Brefeldin A (1,6,7,8,9,11aβ,12,13,14,14αa-Decahydro-1β,13α-dihydroxy-6β-methyl-4H cyclopent(f)oxacyclotridecin-4-one) and Carbenoxolone (3β,20β)-3-(3-Carboxy-1-oxopropoxy)-11-oxoolean-12-en-29-oic acid disodium) were from Sigma-Aldrich.

Analysis of Ca^{2+} signals

Ca^{2+} signals were quantified by measuring the pixel intensity of region of interest (ROI) corresponding to the individual astrocytes using Fiji ImageJ software (www.fiji.sc, RRID:SCR_002285). Normalized changes in Fluo-4 AM fluorescence were expressed as $\Delta F/F = (F - F_0)/F_0$, i.e. the difference between Fluo-4 signal (F) and baseline Fluo-4 fluorescence (F_0), divided by F_0. ROIs were established based on the morphology of astrocytes observed in response to ATP. Astrocyte Ca^{2+} signals were defined as immune cell-evoked if the change in F relative to F_0 was greater than 3 × s.d. of the baseline signal for at least 5 s and these glial cells are named responders. To compare the magnitude of Ca^{2+} signals evoked by immune cells with the baseline Ca^{2+} signals without biased selection of the threshold values, we integrated the consecutive $\Delta F/F_0$ signals as follows: 100 s before and 100 s from the start of immune cell application. Experimental values are expressed as $\Delta F/F0 \cdot s$ in all graphs. Areas of all the $\Delta F/F_0$ signals were calculated in Clampfit software, V11.0.3 (www.moleculardevices.com, RRID:SCR_011323).

ATP measurement

ATP release from Peripheral IC and CNS IIC was measured using a luciferin-luciferase assay ATPLite kit as described in manufacturer protocol (PerkinElmer, Boston, USA), and bioluminescence was quantified using a Chameleon plate reader (Cole-Parmer, IL, USA). Peripheral IC and CNS IIC were maintained under the same conditions. Prior to experiments the cells were centrifuged at 500 × g and resuspended in ECS. The same number of Peripheral IC and CNS IIC (50 000 cells each per well) were placed in 96-well dark plate. Absolute values of extracellular ATP were obtained from ATP standards prepared on the day of the experiment and measured at the same time as samples.

Immunohistochemistry and analysis

For confocal microscopy EAE rats were deeply anesthetized with Zoletil®50 (Virbac; 30 mg/kg i.p) and transcardially perfused with 0.9% NaCl. Perfused spinal cords were dissected, and lumbar parts further processed: fixation (4% PFA (Sigma-Aldrich) in 0.1 M PBS, pH 7.4 overnight at 4 °C) and cryoprotection (increasing concentrations of sucrose (Sigma-Aldrich) solutions, 10-30% in 0.1 M PBS, pH 7.4). Tissues were frozen in 2-methylbutane and stored at -80 °C. 20 µm thick transverse sections were cut using a cryostat. Before immunostaining sections were 3x rinsed in PBS. Then to prevent binding of antibodies to non-specific epitopes, sections were incubated for 30 min at room temperature in a blocking solution containing Normal Donkey Serum (10% in PBS; Santa Cruz Biotechnology, Cat# sc-2044, RRID:AB_10188561). For immunolabeling, sections were incubated with primary antibodies overnight at 4 ºC. After rinsing at room temperature with PBS 3x for 5 min each, sections were incubated with a secondary antibodies for 2 h at room temperature. After rinsing 3x in PBS, sections were mounted on glass-slides and coversliped in Mowiol (Calbiochem, Millipore, Darmstadt, Germany). Primary antibodies used: mouse anti-CD4 (1:200, Sigma-Aldrich, Cat# SAB4700733, RRID:AB_2828023), rabbit anti-GFAP (Glial Fibrillary Acidic Protein, 1:400, Agilent, Cat# Z0334, RRID:AB_10013382). Secondary antibodies: donkey anti-mouse Alexa Fluor 568 (1:250; Thermo Fisher Scientific Cat# A10037, RRID:AB_2534013), donkey anti-rabbit Alexa Fluor 488 (1:250, Thermo Fisher Scientific, Cat# A-21206, RRID:AB_2535792). Sections were first immunolabeled with antibody against CD4 and afterwards against GFAP. Sections incubated with appropriate secondary antibodies without the primary antibodies were

used as negative controls. Images were acquired using a Leica DMI 6000 confocal microscope (TCS SP5 II, Leica Microsystems, Wetzlar, Germany).

Images were processed with Fiji ImageJ software. 3-4 spinal cord sections were imaged and analyzed per animal. The number of infiltrated $CD4^+$ T cells in the spinal cord was manually counted in the white and grey matter from the images representing maximum intensity projections having a z step size of 0.9 µm. Proximity analysis of the interaction between $CD4^+$ T cells and GFAP immunolabeled astrocytes in the white and grey matter was next performed. On the basis of CD4 staining, $CD4^+$ T cells were identified as small spheres of approximately 6 µm diameter. Analysis was done on the maximum z-projection (6.3 µm z-stack) consisting of 7 consecutive planes with z step size of 0.9 µm: 3 planes above and below the focal plane of the $CD4^+$ T cell. The same planes of GFAP signal were used for analysis. The ROI was established according to the size of $CD4^+$ T cell. Then the radial distance between the center of the ROI and intersection with GFAP signal in the 0.5 µm step size up to 10 µm radius was automatically measured using Sholl analysis plugin of Fiji ImageJ software (https://imagej.net/Sholl_Analysis). Cells were considered to interact if the intersection with GFAP signal was detected at the ROI border ($CD4^+$ T cell surface), measured 3 µm from the ROI center. The number of $CD4^+$ T cells was counted manually from each section analyzed.

Statistical analyses

Data were analyzed and plotted using SigmaPlot Software, V11.0 (www.sigmaplot.com/products/sigmaplot/, RRID:SCR_003210) and GraphPad Prism Software, V6.01 (www.graphpad.com/, RRID:SCR_002798). No data were removed prior to statistical analysis. All datasets were tested for Gaussian distribution with the Kolmogorov-Smirnov normality test. If compared datasets passed the normality and equal-variance tests, a two-tailed unpaired Student's t test was used to compare the significance difference in the means between the two groups, otherwise a nonparametric Mann-Whitney test was chosen. When experiments were performed on the same cell, then a Paired two-tailed Student's t test (for data that passed normality test) or nonparametric Wilcoxon Signed Rank test (for data that did not pass normality test) were carried out. For multiple group datasets that did not pass normality test, one-way ANOVA analysis on Ranks was used (Kruskal-Wallis test), followed by Dunn's post hoc test for multiple comparisons of means of datasets of unequal size. Full reports of statistical tests used to

365 measure significance, along with the corresponding significance levels (*P* value), are indicated in
366 figures and figure legends. *P* values were considered significant if they were less than 0.05. All
367 experimental conditions were repeated with CNS IIC that were isolated from at least three
368 animals with EAE. CNS IIC effects were replicated in at least three independent experiments
369 conducted on minimum two different astrocyte culture preparations, and number of independent
370 experiments for each experimental condition is reported in figure legends. n represents number
371 of astrocytes, while N represents number of animals with EAE in experiments, and their exact
372 values are given in Figures and Figure legends. An estimate of the sample size needed for most
373 of the conducted experiments is as follows: for a control response of 100% (i.e. in the presence
374 of CNS IIC), a typical response SD of 40%, a response in a specific experimental condition of
375 30% (with various drugs), a power of 80% and $P < 0.05$, seven astrocytes per coverslip are
376 needed (http://www.biomath.info/power/ttest.htm) in each of the experimental groups. The exact
377 numbers depend on the drug effect size and standard deviation of data. Data are presented as
378 mean ± SD scatter plots, and box and whisker plots. In box plots central line shows the median,
379 central dot shows the mean, the edges of the box define the upper and lower quartile values, and
380 whiskers show the minimum-maximum range. Figures were made with CorelDRAW Graphics
381 Suite Software, V14.0 (www.coreldraw.com, RRID:SCR_014235).
382
383 # Results
384
385 ## CNS IIC induce Ca^{2+} elevation in astrocytes

386 Continuous cross-talk between the cells in the CNS present challenges for defining astrocyte
387 Ca^{2+} dynamics during specific interaction with the CNS IIC. To achieve unambiguous astrocyte-
388 immune cell interaction analysis, we used an experimental system in which we monitored Ca^{2+}
389 level of cultured naïve spinal cord astrocytes in response to the brief bath application of the CNS
390 IIC isolated from the spinal cord of rats with EAE (Figure 1a). Rats developed an acute
391 monophasic EAE characterized by severe limb paralysis as previously described by (Miljković et
392 al., 2011b), and CNS IIC were obtained when animals were at the late onset or at the peak of
393 disease. These CNS IIC isolates contain different immune cell populations, predominantly $CD4^+$
394 T cells, that were recruited from the periphery into the CNS during EAE (Miljković et al.,

2011a). To visualize and track intracellular Ca^{2+} dynamics of astrocytes in pure culture (Figure S1), we used cell-permeable fluorescent Ca^{2+} indicator Fluo-4. Initially, we monitored astrocyte Ca^{2+} level in response to the application of the CNS IIC at increasing concentrations, in the range of those reported for the pathological state of EAE (Schläger et al., 2016). We found that CNS IIC applied at the concentration of 5×10^3 cells/ml triggered a small Ca^{2+} elevation in minority of monitored astrocytes, whereas application at increasing concentrations of 25×10^3 cells/ml and 50×10^3 cells/ml evoked robust Ca^{2+} elevations in numerous astrocytes (Figure 1b). The magnitude of astroglial Ca^{2+} change increased with rising CNS IIC concentrations (Figure 1c), indicating that Ca^{2+} signals mediate astrocyte interaction with the CNS IIC. A more moderate concentration of 25×10^3 cells/ml of CNS IIC that was sufficient to trigger prominent Ca^{2+} increase in vast majority of astrocytes, was used in further experiments.

To determine if astrocyte Ca^{2+} increase is triggered specifically by the immune cells infiltrated in the CNS, we next subjected astrocytes to the immune cells isolated from the cervical lymph node of EAE rat (Peripheral IC). Time-lapse Ca^{2+} imaging revealed a striking difference between astrocyte responsiveness to the immune cells: astrocytes did not exhibit a Ca^{2+} change in response to the Peripheral IC application, while they responded to the subsequently applied CNS IIC with a large Ca^{2+} elevation (Figure 1d-1f). These CNS IIC-evoked Ca^{2+} transients exhibited similar waveforms, began at the onset delay of 11.312 ± 6.760 s (mean ± SD, n = 32 astrocytes) and persisted for many seconds after the cessation of CNS IIC application. Moreover, astrocytes exhibited a large and stable Ca^{2+} increases in response to the consecutive CNS IIC applications (Figures 1g, 1h), indicating that interaction between astrocytes and CNS IIC is consistent. In addition, CNS IIC isolated from EAE rats of both sexes triggered Ca^{2+} responses in a comparable number of astrocytes, and similarly enhanced astroglial Ca^{2+} (Figure S2), suggesting that sex difference does not affect the ability of CNS IIC to stimulate Ca^{2+} elevation in astrocytes in our experimental system.

To assess whether astrocyte Ca^{2+} increase is evoked by the CNS IIC or immune cells-derived soluble factors which define a significant part of immune cell intercellular signaling in the CNS autoimmunity (Goverman, 2009; Mayo et al., 2012), we next monitored Ca^{2+} dynamics of astroglia during application of the CNS IIC or their conditioned medium (Figure 1i). Removal of the CNS IIC and application of the CNS IIC-conditioned medium promoted Ca^{2+} change in

minority of astrocytes, relative to the CNS IIC presence in the matched interleaved control triggering Ca^{2+} increase in numerous glial cells (Figure 1j). Moreover, astrocytes in which we detected a response in the CNS IIC-conditioned medium had a 52% smaller Ca^{2+} elevation than that evoked when the CNS IIC were present (Figure 1k). These results indicate that CNS IIC in close proximity to astrocytes dominate a rapid intracellular Ca^{2+} increase in these glial cells.

CNS IIC-induced increase in astrocyte Ca^{2+} does not require metabotropic glutamate receptors or TRPA1

Many mechanisms leading to an intracellular Ca^{2+} increase in astrocytes have been described. An important role has been assigned to the metabotropic group I receptors for glutamate (mGluR1 and mGluR5), a G-protein coupled receptors that liberate Ca^{2+} from internal stores (Araque et al., 2014). A non-selective transient receptor potential A1 (TRPA1) cation channels have also been implicated in contributing to the astroglial Ca^{2+} increase by regulating Ca^{2+} influx into the astrocytes (Shigetomi et al., 2013). We assessed whether inhibition of these plasma membrane proteins on astrocytes attenuated Ca^{2+} change induced by the CNS IIC application (Figure 2a). However, in our experiments CNS IIC-triggered astrocytic Ca^{2+} changes were not affected by bath applied blockers of mGluR1 (blocked by 100 μM CPCCOEt; Fig. 2b-2d) and mGluR5 receptors (blocked by 50 μM MPEP; Figure 2e-2h), or the TRPA1 blocker A967079 (10 μM; Figure 2i-2k). Astrocytes displayed robust transient Ca^{2+} increases in response to the CNS IIC application as those we measured in the interleaved Control experiments without the blockers (Figure 2d, 2h, 2k). Furthermore, blockers of tested receptors and channels did not alter the proportion of responding astrocytes relative to their interleaved Controls (Figure 2b, 2f, 2i). These results indicate that CNS IIC-evoked increase in astroglial Ca^{2+} is a phenomenon that does not result from the activation of mGluR1, mGluR5 or TRPA1, and that there is another mechanism that enables Ca^{2+} change in these glial cells.

CNS IIC induce Ca^{2+} elevation in astrocytes via P2X7 receptor activation

Purinergic signaling is the most widespread mean of astroglial intercellular communication (Butt, 2011). In addition, astrocyte response to the pathophysiological stimuli is often associated with a intracellular Ca^{2+} increase mediated by the P2 purinergic receptors (Franke et al., 2012),

raising the possibility that these receptors may contribute to the CNS IIC-induced Ca^{2+} elevation in astrocytes. To explore this possibility, we next blocked purinergic receptors on astrocytes and monitored the response of glial cells to the CNS IIC application (Figure 3a). Blocking glial P2 receptors with a non-selective blocker PPADS (50 μM) strongly reduced the proportion of astrocytes that responded to the applied CNS IIC by 56% (Figure 3b). Moreover, the fraction of astrocytes in which we detected a Ca^{2+} change with PPADS present, had a 60% smaller Ca^{2+} elevation relative to the interleaved Control (Figure 3c, 3d), indicating that purinergic receptors participate in the CNS IIC-induced Ca^{2+} change in astroglial cells. To define the receptor subtypes responsible, in the next experiments we applied selective purinoreceptor antagonists to astrocytes. Blocking metabotropic G-protein coupled P2Y1 receptors, a highly potent stimulant of Ca^{2+} release from intracellular stores (Butt, 2011) with MRS 2179 (10 μM), however, did not affect CNS IIC-induced astroglial Ca^{2+} increase, and the proportion of astrocytes responding to the CNS IIC application was the same as in the interleaved Control (Figure 3e-3g). Previous studies have implicated P2X7 receptors as an important component of astroglial response to the inflammatory conditions in MS (Narcisse et al., 2005; Amadio et al., 2017). Given that P2X7 receptors are ATP-gated cation channels controlling Ca^{2+} entry into astrocytes (Fumagalli et al., 2003; Hamilton et al., 2008), we next determined whether this receptor type plays a role in regulating astroglial Ca^{2+} dynamics during interaction with the CNS IIC. Block of the P2X7 receptors with A438079 (10 μM), reduced the proportion of astrocytes that responded to the CNS IIC application by 72%, and Ca^{2+} change of a few cells detected in this antagonist was 74% smaller relative to that measured in the interleaved Control (Figure 3h-3j). Short application of BzATP at a low concentration (5 μM, for 5 s) (Khadra et al., 2013), an agonist of P2X7 receptors, produced P2X7 receptor-dependent transient Ca^{2+} increase in astrocytes similar to that triggered by the CNS IIC (Figure 3k, 3l). Together, these results indicate that CNS IIC-induced Ca^{2+} increase in astrocytes occurs primarily due to the activation of astroglial P2X7 receptors.

CNS IIC-induced P2X7 receptor activation and Ca^{2+} increase in astrocytes depend on astroglial hemichannels

Astrocytes are the main source of ATP in the CNS (Franke et al., 2012), but immune cells can also release this purine (Burnstock and Boeynaems, 2014), creating new challenges for

assessment of the mechanism of P2X7 receptor-mediated astroglial Ca^{2+} increase induced by the CNS IIC. To determine if the CNS IIC-derived ATP activates glial P2X7 receptors, we next quantified release of this purine from the CNS IIC and the Peripheral IC using luciferin-luciferase chemiluminescence bioassay (Figure 4a). Given previous reports of increased ATP secretion from activated immune cells (Schenk et al., 2008; Ledderose et al., 2018; Dosch et al., 2019), and the complete absence of astrocyte response to the Peripheral IC application (see Figure 1e), we predicted that CNS IIC would activate astroglial purinergic receptors by releasing more ATP. Unexpectedly, concentration of extracellular ATP released by the CNS IIC was similar to that measured for the Peripheral IC (Figure 4a), suggesting that immune cell-derived ATP did not induce P2X7 receptor activation in astrocytes.

Astrocyte-derived ATP has been shown to act as a signaling molecule which activates purinergic receptors in an autocrine or paracrine manner (Figueiredo et al., 2014; Shen et al., 2017; Nikolic et al., 2018), providing a means to assess this role of astroglial ATP in activating P2X7 receptors during interaction with CNS IIC. To achieve this assessment, in the following experiments we disrupted mechanisms of ATP release from astrocytes (Figure 4b). To inhibit vesicular ATP release, we incubated glial cells in brefeldin A (Bref. A, 2 μg/ml). Although this manipulation has been reported to inhibit ATP-dependent Ca^{2+} elevation in astrocytes (Bowser and Khakh, 2007), astrocyte response to the CNS IIC application persisted, with the proportion of responding glial cells and average magnitude of their Ca^{2+} change unaltered relative to the interleaved control (Figure 4c-4e). In marked contrast, carbenoxolone (CBX, 50 μM) which inhibits release of ATP through the astrocytic hemichannels (Kang et al., 2008; Chever et al., 2014; Delekate et al., 2014), reduced the proportion of responding astrocytes by 56%, and reduced the magnitude of their Ca^{2+} increase by 65%, relative to the CNS IIC effect in the interleaved Control (Figure 4f-4h). Of note, CBX did not prevent Ca^{2+} response of astrocytes to the subsequently applied ATP, indicating that glial ability to react to ATP was not affected by this inhibitor (Figure 4i). Together, these results support the conclusion that CNS IIC application promotes astroglial hemichannel-controlled ATP release which then activates P2X7 receptors and causes increase in cytosolic Ca^{2+} in astrocytes.

CNS infiltrated $CD4^+$ T cells increase astroglial Ca^{2+} activity and interact with astrocytes during EAE

$CD4^+$ T cells mainly constitute CNS IIC isolate (Miljković et al., 2011a), and are recognized to be critical for the establishment and perpetuation of EAE (McFarland and Martin, 2007), providing a means to determine whether CNS IIC-induced Ca^{2+} increase in astrocytes is specifically $CD4^+$ T cell-associated. To assess this effect, we next purified $CD4^+$ CNS infiltrated T cells ($CD4^+$ CNS ITC) from the rest of the CNS IIC population (CNS IIC without $CD4^+$ ITC) isolated from the spinal cord of EAE rat, and monitored astrocyte Ca^{2+} level upon application of these two groups of CNS IIC. The proportion of $CD4^+$ CNS ITC measured by the flow cytofluorometry (40.916% ± 11.156%, mean ± SD, N = 6 EAE rats, 6 independent measurements), constituted approximately half of the CNS IIC population, thus, we applied $CD4^+$ CNS ITC and CNS IIC without $CD4^+$ ITC at the same 25×10^3 cells/ml concentration, which we found to induce reliable Ca^{2+} increase in astrocytes (see Figure 1h). Remarkably, $CD4^+$ CNS ITC application evoked a vigorous Ca^{2+} increase in a majority of monitored astrocytes, whereas subsequently applied CNS IIC without $CD4^+$ ITC induced Ca^{2+} change in a minor portion of the glial cells (Figure 5a, 5b). Notably, Ca^{2+} increase in astrocytes induced by the $CD4^+$ CNS ITC was 9.1× higher relative to that detected with the CNS IIC without $CD4^+$ ITC (Figure 5c). Indeed, astrocytes displayed robust Ca^{2+} increase in the presence of $CD4^+$ CNS ITC that was remarkably similar to the Ca^{2+} elevation observed in the interleaved Control experiment when the total population of the CNS IIC was applied (Figure 5c). Together, these results indicate that autoreactive $CD4^+$ T cells are sufficient to induce Ca^{2+} increase in astroglial cells.

Infiltrated $CD4^+$ T cells have been shown to exhibit random walk behavior in EAE (Schläger et al., 2016) and they may often interact with astrocytes in situ, accounting for the abundance of these glial cells and their almost complete coverage of the CNS. To visualize spatial distribution of $CD4^+$ T cells relative to astrocytes, we performed immunolabeling of these two cell types in the spinal cord of EAE rat. Immunolabeled $CD4^+$ T cells were scattered deeply in the spinal cord parenchyma and neighbored by the meshwork of astrocytes immunostained for GFAP (Figure S3). By using proximity analysis we found that a substantial portion of the CNS infiltrated $CD4^+$ T cells interact with a GFAP labeled astrocytes during EAE (Figure 5d, 5e). These results

suggest that interaction between astrocytes and $CD4^+$ T cells in the glial local environment occurs in the inflamed CNS, as indicated by our Ca^{2+} imaging data.

Discussion

This work shows that Ca^{2+} signals mediate rapid astroglial interaction with the CNS IIC. We reveal here that brief application of autoreactive immune cells isolated from the CNS of rat with EAE induces a rapid purinergic receptor-dependent Ca^{2+} elevation in cultured naïve astrocytes.

In the setting of autoimmune inflammatory disease such as MS, interactions between many cell types of the immune and CNS systems create an inflammatory CNS environment that drives demyelination rendering neurons susceptible to degeneration. These interactions occur between immune cells and glial cells, including astrocytes (Kang et al., 2010; Mayo et al., 2014, 2016), microglia (Carson, 2002; Heppner et al., 2005) or oligodendrocyte precursor cells (Kirby et al., 2019). In addition, astrocytes engage in interaction with oligodendrocyte progenitors and microglia in this disease, a cellular dialogues through which astrocytes can promote inhibition of remyelination (Kirby et al., 2019), and gain ability to induce the death of neurons (Liddelow et al., 2017). Because of these complex astroglial interactions with many cell types, it is difficult to obtain an insight into the astroglial activity pattern specifically in response to the autoreactive immune cells which are considered to mediate early steps of MS and EAE pathology (McFarland and Martin, 2007). To overcome these limitations, we performed imaging of cultured astrocytes Ca^{2+} dynamics upon application of the CNS IIC isolated from the rat with EAE, allowing visualization of the CNS IIC-evoked changes in astroglial activity pattern on a fast time scale.

Astrocytes exhibit dynamic changes in their activity and structure on a temporal scale that spans several orders of magnitude, from miliseconds to days, enabling them to respond to the requirements of their environment in physiological and pathological conditions (Anderson et al., 2014; Nimmerjahn and Bergles, 2015). In EAE, immune cell-derived inflammatory mediators have been shown to induce profound changes in the expression of inflammation-associated genes in astrocytes (Qian et al., 2007; Mayo et al., 2016; Prajeeth et al., 2017). These changes induced by the inflammatory factors are commonly associated with a long-lasting astroglial modifications that involve cellular hypertrophy and proliferation (e.g. reactive astrogliosis) (Anderson et al., 2014). Our studies indicate that immune cell-astrocyte interaction can also occur on a faster time

574 scale. By imaging intracellular Ca^{2+} in astrocytes we reveal that autoreactive CNS IIC and not
575 the Peripheral IC in close proximity to astrocytes within seconds induce a robust and transient
576 astroglial Ca^{2+} elevation. Our results also reveal that this interaction is consistent, and indicate
577 that astrocytes would exhibit a transient Ca^{2+} increase each time they encounter autoreactive
578 immune cells in their local environment. Moreover, we show that astroglial Ca^{2+} increase is
579 primarily induced by the application of autoreactive $CD4^+$ T cells, an immune cell type that has a
580 critical role in pathogenesis of CNS autoimmunity (Goverman, 2009), and astrocyte-$CD4^+$ T cell
581 interaction appears to be effective in the spinal cord of rat with EAE. Together, these results
582 indicate that in addition to the immune cell-promoted long-lasting phenotypic changes in
583 astrocytes in EAE (Brambilla, 2019), autoreactive immune cells can evoke a rapid change in the
584 fundamental, Ca^{2+} based aspect of astrocyte physiology.

585 CNS IIC-induced Ca^{2+} increase in astrocytes was markedly attenuated after the specific block of
586 P2X7 receptors, and was mimicked by the stimulation of this glial receptor with a low
587 concentration of agonist, suggesting that P2X7 receptor-dependent signaling primarily mediates
588 CNS IIC-astrocyte interaction in our studies. Our data also reveal that activation of P2X7
589 receptors is regulated mainly within astrocytes, because blocking the hemichannel-dependent
590 ATP release in these glial cells strongly reduced Ca^{2+} increase induced by the CNS IIC
591 application. Of note, Ca^{2+} increase in astrocytes was detected ~10 s after the onset of the CNS
592 IIC application, presumably reflecting the steps required to promote ATP release from
593 hemichannels to activate P2X7 receptors on astrocytes. These initial steps remain unknown but
594 may be mediated by integrins, adhesion molecules mediating cell-cell communication that are
595 upregulated on T cells infiltrated into the CNS in MS and EAE (Archelos et al., 1999). Indeed,
596 integrin engagement has been linked to the astrocyte P2X7 receptor activation (Henríquez et al.,
597 2011) by the hemichannel-derived ATP and to the subsequent increase in the intracellular Ca^{2+} in
598 these glial cells (Alvarez et al., 2016). Our data conclusively demonstrate that P2X7 receptor-
599 dependent signaling dominates CNS IIC-induced Ca^{2+} elevation in astrocytes. This could
600 contribute to the release of signaling molecules from astrocytes and accelerate neurodegenerative
601 processes in CNS autoimmunity. Indeed, activation of astroglial P2X7 receptors is closely
602 associated with a downstream cytokine, glutamate and reactive oxygen species release from
603 astrocytes, a processes that drive neuroinflammation and neuronal damage (Burnstock and
604 Knight, 2018).

605 Our data indicate that astrocyte interaction with the immune cells infiltrated into the CNS shares
606 some key features of the signaling these glial cells utilize to communicate with their CNS-
607 resident neighbors, namely the increase in intracellular Ca^{2+} regulated by purinergic receptor
608 activation. Indeed, purine-mediated signaling has been considered to be a dominant form of
609 astrocyte intercellular communication in the CNS, by virtue of these cells to release purines to
610 modulate neuronal activity, to communicate among each other and with other types of glia
611 (Fields and Burnstock, 2006; Butt, 2011). Moreover, purine-mediated astroglial signaling is
612 enhanced in pathological states such as epilepsy (Alvarez-Ferradas et al., 2015), Alzheimer's
613 disease (Delekate et al., 2014) or cerebral ischemia (Kuboyama et al., 2011). In MS, increase in
614 the expression of P2X7 receptor has been observed in hypertrophic astrocytes in the frontal
615 cortex parenchyma of MS patients (Amadio et al., 2017), and our data suggest that signaling
616 mediated by this purinergic receptor may be important for astrocyte intercellular communication
617 with a nearby autoreactive immune cells in CNS autoimmunity.

618 Essential aspects of the intracellular Ca^{2+} signals described in cultured astrocytes (Cornell-Bell et
619 al., 1990), have been substantiated in acute brain slices (Porter and McCarthy, 1996), as well as
620 in vivo (Hirase et al., 2004; Wang et al., 2006). However, caution should be exercised in
621 extrapolating the results of this study to EAE and MS. We have shown that CNS IIC-induced
622 astroglial response is rapid and consistent, leading us to favor the idea that in the inflamed CNS,
623 CNS IIC in astroglial local environment may frequently induce Ca^{2+} increase in these glial cells.
624 A part of astroglial response is most likely mediated by the CNS IIC-derived inflammatory
625 mediators. Indeed, we have observed that application of the CNS IIC-conditioned medium
626 induced Ca^{2+} increase in a minor fraction of glial cells and of a lower magnitude, and previous
627 studies have shown that astrocytes exhibit Ca^{2+} elevation in response to the application of
628 inflammatory cytokines (Domercq et al., 2006; Nikolic et al., 2018). However, we do not rule
629 out the possibility that astrocyte-immune cell interaction revealed in these studies may be shaped
630 by the inputs from other cells in the neuroinflammatory CNS environment, predominantly that
631 from activated microglia. Indeed, proinflammatory cytokines derived from activated microglia
632 can affect not only the response of the CNS infiltrating $CD4^+$ T cells in EAE by regulating their
633 expansion and differentiation (Li et al., 2003; Dong and Yong, 2019), but can also promote
634 neurotoxic astroglial activity in MS (Liddelow et al., 2017). Consequently, the net effect of these
635 microglial inputs on the astrocyte-immune cell interaction in EAE is difficult to predict. Future

studies involving selective manipulation of individual cell type's activities will help to clarify the actual outcome of this intercellular crosstalk on the immune cell-induced astrocyte Ca^{2+} signalling in CNS autoimmunity.

Our studies have focused primarily on understanding of the CNS IIC effect on astroglial pattern of activity which is important to understand how astrocytes respond to the autoreactive immune cells present in their local environment in CNS autoimmunity. Our results establish a sequence of events that control CNS IIC-evoked rapid Ca^{2+} increase in astrocytes, and offer new conceptual framework for studying astrocyte-immune cell interaction in CNS autoimmunity. Further studies will help define the roles of these astroglial Ca^{2+} changes with early and persistent neurodegenerative processes in EAE. This analysis may reveal new strategies for ameliorating neuroinflammation in an autoimmune disease.

Conflict of interest statement

No conflict of interest, financial or otherwise, is declared by the authors.

Author contributions

All authors had full access to all of the data in the study and take responsibility for the integrity of the data. All authors approved final version of the manuscript. *Conceptualization*, Lj.N.; *Methodology*, M.M., P.R.A., Dj.M. and Lj.N.; *Investigation*, D.B., K.M., M.L., M.M., J.B.P. and D.S.; *Formal Analysis*, M.L., M.M., J.B.P. and Lj.N.; *Resources*: P.R.A., Dj.M., B.P., and Lj.N.; *Writing – Original Draft*, J.B.P. and Lj.N.; *Writing – Review & Editing*, D.B., K.M., M.L., M.M., J.B.P., D.S., B.P., P.R.A., Dj.M., and Lj.N.; *Visualization,* Lj.N.; *Supervision,* Dj.M. and Lj.N.; *Funding Acquisition,* P.R.A., Dj.M., B.P. and Lj.N.

Acknowledgments

We thank Dr. Etienne Audinat for critical reading of the manuscript, Dr. Danijela Bataveljic for inputs during experimental work, Goran Djmura and Milijana Vasiljevska for maintaining and providing Dark Agouti rats, Dr. Nataša Nestorović for technical help with confocal imaging, and to Dr. Bojan Jevtić for help with immune cell purification. This work was supported by Ministry

of Education, Science and Technological Development of Republic of Serbia (Contract no. 451-03-68/2020-14/200007, 451-03-68/2020-14/200178, 451-03-68/2020-14/200053), and a Fellowship *Start up for Science* from the Centre for Leadership Development to Lj.N.

Data Accessibility Statement

The data that support the findings of this study are available from the corresponding author upon reasonable request.

References

Alvarez-Ferradas C, Morales JC, Wellmann M, Nualart F, Roncagliolo M, Fuenzalida M, Bonansco C. 2015. Enhanced astroglial Ca2+ signaling increases excitatory synaptic strength in the epileptic brain. Glia 63:1507–1521.

Alvarez A, Lagos-Cabré R, Kong M, Cárdenas A, Burgos-Bravo F, Schneider P, Quest AFG, Leyton L. 2016. Integrin-mediated transactivation of P2X7R via hemichannel-dependent ATP release stimulates astrocyte migration. Biochim Biophys Acta - Mol Cell Res [Internet] 1863:2175–2188. Available from: http://dx.doi.org/10.1016/j.bbamcr.2016.05.018

Amadio S, Parisi C, Piras E, Fabbrizio P, Apolloni S, Montilli C, Luchetti S, Ruggieri S, Gasperini C, Laghi-Pasini F, Battistini L, Volonté C. 2017. Modulation of P2X7 receptor during inflammation in multiple sclerosis. Front Immunol 8:1–17.

Anderson MA, Ao Y, Sofroniew M V. 2014. Heterogeneity of reactive astrocytes. Neurosci Lett [Internet] 565:23–29. Available from: http://dx.doi.org/10.1016/j.neulet.2013.12.030

Araque A, Carmignoto G, Haydon PG, Oliet SHR, Robitaille R, Volterra A. 2014. Gliotransmitters travel in time and space. Neuron 81:728–739.

Archelos JJ, Previtali SC, Hartung HP. 1999. The role of integrins in immune-mediated diseases of the nervous system. Trends Neurosci 22:30–38.

Baecher-Allan C, Kaskow BJ, Weiner HL. 2018. Multiple Sclerosis: Mechanisms and Immunotherapy. Neuron [Internet] 97:742–768. Available from: https://doi.org/10.1016/j.neuron.2018.01.021

Bazargani N, Attwell D. 2016. Astrocyte calcium signaling: the third wave. Nat Neurosci 19:182–189.

695 Bowser DN, Khakh BS. 2007. Vesicular ATP Is the Predominant Cause of Intercellular Calcium
696 Waves in Astrocytes. J Gen Physiol 129:485–491.
697 Brambilla R. 2019. The contribution of astrocytes to the neuroinflammatory response in multiple
698 sclerosis and experimental autoimmune encephalomyelitis. Acta Neuropathol [Internet].
699 Available from: http://link.springer.com/10.1007/s00401-019-01980-7
700 Burnstock G, Boeynaems JM. 2014. Purinergic signalling and immune cells. Purinergic Signal
701 10:529–564.
702 Burnstock G, Knight GE. 2018. The potential of P2X7 receptors as a therapeutic target,
703 including inflammation and tumour progression. Purinergic Signal 14:1–18.
704 Butt AM. 2011. ATP: A ubiquitous gliotransmitter integrating neuron-glial networks. Semin Cell
705 Dev Biol [Internet] 22:205–213. Available from:
706 http://dx.doi.org/10.1016/j.semcdb.2011.02.023
707 Carson MJ. 2002. Microglia as liaisons between the immune and central nervous systems:
708 Functional implications for multiple sclerosis. Glia 40:218–231.
709 Chever O, Lee C-Y, Rouach N. 2014. Astroglial Connexin43 Hemichannels Tune Basal
710 Excitatory Synaptic Transmission. J Neurosci 34:11228–11232.
711 Colombo E, Farina C. 2016. Astrocytes: Key Regulators of Neuroinflammation. Trends
712 Immunol 37:608–620.
713 Cornell-Bell AH, Finkbeiner SM, Cooper MS, Smith SJ. 1990. Glutamate induces calcium
714 waves in cultured astrocytes: long-range glial signaling. Science 247:470–473.
715 Delekate A, Füchtemeier M, Schumacher T, Ulbrich C, Foddis M, Petzold GC. 2014.
716 Metabotropic P2Y1 receptor signalling mediates astrocytic hyperactivity in vivo in an
717 Alzheimer's disease mouse model. Nat Commun [Internet] 5:5422. Available from:
718 http://www.nature.com/doifinder/10.1038/ncomms6422
719 Dendrou CA, Fugger L, Friese MA. 2015. Immunopathology of multiple sclerosis. Nat Rev
720 Immunol [Internet] 15:545–558. Available from: http://dx.doi.org/10.1038/nri3871
721 Domercq M, Brambilla L, Pilati E, Marchaland J, Volterra A, Bezzi P. 2006. P2Y1 receptor-
722 evoked glutamate exocytosis from astrocytes: Control by tumor necrosis factor-?? and
723 prostaglandins. J Biol Chem 281:30684–30696.
724 Dong Y, Yong VW. 2019. When encephalitogenic T cells collaborate with microglia in multiple
725 sclerosis. Nat Rev Neurol [Internet] 15:704–717. Available from:

726 http://dx.doi.org/10.1038/s41582-019-0253-6
727 Dosch M, Zindel J, Jebbawi F, Melin N, Sanchez-Taltavull D, Stroka D, Candinas D, Beldi G.
728 2019. Connexin-43-dependent ATP release mediates macrophage activation during sepsis.
729 Elife 8:1–24.
730 Fields RD, Burnstock G. 2006. Purinergic signalling in neuron-glia interactions. Nat Rev
731 Neurosci 7:423–436.
732 Figueiredo M, Lane S, Stout RF, Liu B, Parpura V, Teschemacher AG, Kasparov S. 2014.
733 Comparative analysis of optogenetic actuators in cultured astrocytes. Cell Calcium
734 [Internet] 56:208–214. Available from: http://dx.doi.org/10.1016/j.ceca.2014.07.007
735 Franke H, Verkhratsky A, Burnstock G, Illes P. 2012. Pathophysiology of astroglial purinergic
736 signalling. Purinergic Signal 8:629–657.
737 Fumagalli M, Brambilla R, D'Ambrosi N, Volonté C, Matteoli M, Verderio C, Abbracchio MP.
738 2003. Nucleotide-mediated calcium signaling in rat cortical astrocytes: Role of P2X and
739 P2Y receptors. Glia 43:218–230.
740 Goverman J. 2009. Autoimmune T cell responses in the central nervous system. Nat Rev
741 Immunol 9:393–407.
742 Hamilton N, Vayro S, Kirchhoff F, Verkhratsky A, Robbins J, Gorecki DC, Butt AM. 2008.
743 Mechanisms of ATP- and glutamate-mediated calcium signaling in white matter astrocytes.
744 Glia 56:734–749.
745 Haydon PG. 2001. GLIA: listening and talking to the synapse. Nat Rev Neurosci 2:185–193.
746 Henríquez M, Herrera-Molina R, Valdivia A, Alvarez A, Kong M, Muñoz N, Eisner V,
747 Jaimovich E, Schneider P, Quest AFG, Leyton L. 2011. ATP release due to Thy-1-integrin
748 binding induces P2X7-mediated calcium entry required for focal adhesion formation. J Cell
749 Sci 124:1581–1588.
750 Heppner FL, Greter M, Marino D, Falsig J, Raivich G, Hövelmeyer N, Waisman A, Rülicke T,
751 Prinz M, Priller J, Becher B, Aguzzi A. 2005. Experimental autoimmune encephalomyelitis
752 repressed by microglial paralysis. Nat Med 11:146–152.
753 Hirase H, Qian L, Bartho P, Buzsaki G. 2004. Calcium dynamics of cortical astrocytic networks
754 in vivo. PLoS Biol 2:E96.
755 Kang J, Kang N, Lovatt D, Torres A, Zhao Z, Lin J, Nedergaard M. 2008. Connexin 43
756 Hemichannels Are Permeable to ATP. J Neurosci 28:4702–4711.

Kang Z, Altuntas CZ, Gulen MF, Liu C, Giltiay N, Qin H, Liu L, Qian W, Ransohoff RM, Bergmann C, Stohlman S, Tuohy VK, Li X. 2010. Astrocyte-Restricted Ablation of Interleukin-17-Induced Act1-Mediated Signaling Ameliorates Autoimmune Encephalomyelitis. Immunity [Internet] 32:414–425. Available from: http://dx.doi.org/10.1016/j.immuni.2010.03.004

Khadra A, Tomić M, Yan Z, Zemkova H, Sherman A, Stojilkovic SS. 2013. Dual gating mechanism and function of P2X7 receptor channels. Biophys J 104:2612–2621.

Kirby L, Jin J, Cardona JG, Smith MD, Martin KA, Wang J, Strasburger H, Herbst L, Alexis M, Karnell J, Davidson T, Dutta R, Goverman J, Bergles D, Calabresi PA. 2019. Oligodendrocyte precursor cells present antigen and are cytotoxic targets in inflammatory demyelination. Nat Commun [Internet] 10:1–20. Available from: http://dx.doi.org/10.1038/s41467-019-11638-3

Kuboyama K, Harada H, Tozaki-Saitoh H, Tsuda M, Ushijima K, Inoue K. 2011. Astrocytic P2Y(1) receptor is involved in the regulation of cytokine/chemokine transcription and cerebral damage in a rat model of cerebral ischemia. J Cereb Blood Flow Metab [Internet] 31:1930–1941. Available from: http://www.ncbi.nlm.nih.gov/pubmed/21487414%5Cnhttp://www.ncbi.nlm.nih.gov/pmc/articles/PMC3185880/pdf/jcbfm201149a.pdf

Ledderose C, Fakhari M, Lederer JA, Robson SC, Visner GA, Junger WG, Liu K, Kondo Y, Slubowski CJ, Dertnig T, Denicoló S, Arbab M, Hubner J, Konrad K. 2018. Purinergic P2X4 receptors and mitochondrial ATP production regulate T cell migration. J Clin Invest [Internet] 128:3583–3594. Available from: https://www.lib.uwo.ca/cgi-bin/ezpauthn.cgi?url=http://search.proquest.com/docview/2105005728?accountid=15115%0Ahttp://vr2pk9sx9w.search.serialssolutions.com?ctx_ver=Z39.88-2004&ctx_enc=info:ofi/enc:UTF-8&rfr_id=info:sid/ProQ%3Anahs&rft_val_fmt=info:ofi/f

Li J, Gran B, Zhang GX, Ventura ES, Siglienti I, Rostami A, Kamoun M. 2003. Differential expression and regulation of IL-23 and IL-12 subunits and receptors in adult mouse microglia. J Neurol Sci 215:95–103.

Liddelow SA, Guttenplan KA, Clarke LE, Bennett FC, Bohlen CJ, Schirmer L, Bennett ML, Münch AE, Chung W-S, Peterson TC, Wilton DK, Frouin A, Napier BA, Panicker N, Kumar M, Buckwalter MS, Rowitch DH, Dawson VL, Dawson TM, Stevens B, Barres BA.

788 2017. Neurotoxic reactive astrocytes are induced by activated microglia. Nature [Internet].
789 Available from: http://www.nature.com/doifinder/10.1038/nature21029
790 Mayo L, Cunha AP Da, Madi A, Beynon V, Yang Z, Alvarez JI, Prat A, Sobel RA, Kobzik L,
791 Lassmann H, Quintana FJ, Weiner HL. 2016. IL-10-dependent Tr1 cells attenuate astrocyte
792 activation and ameliorate chronic central nervous system inflammation. Brain 139:1939–
793 1957.
794 Mayo L, Quintana FJ, Weiner HL. 2012. The innate immune system in demyelinating disease.
795 Immunol Rev 248:170–187.
796 Mayo L, Trauger SA, Blain M, Nadeau M, Patel B, Alvarez JI, Mascanfroni ID, Yeste A,
797 Kivisäkk P, Kallas K, Ellezam B, Bakshi R, Prat A, Antel JP, Weiner HL, Quintana FJ.
798 2014. Regulation of astrocyte activation by glycolipids drives chronic CNS inflammation.
799 Nat Med 20:1147–1156.
800 McFarland HF, Martin R. 2007. Multiple sclerosis: a complicated picture of autoimmunity. Nat
801 Immunol 8:913–919.
802 Miljković D, Momčilović M, Stanojević Ž, Rašić D, Mostarica-Stojković M. 2011a. It is still not
803 for the old iron: Adjuvant effects of carbonyl iron in experimental autoimmune
804 encephalomyelitis induction. J Neurochem 118:205–214.
805 Miljković D, Stanojević Ž, Momcilović M, Odoardi F, Flügel A, Mostarica-Stojković M. 2011b.
806 CXCL12 expression within the CNS contributes to the resistance against experimental
807 autoimmune encephalomyelitis in Albino Oxford rats. Immunobiology 216:979–987.
808 Miljkovic D, Stosic-Grujicic S, Markovic M, Momcilovic M, Ramic Z, Maksimovic-Ivanic D,
809 Mijatovic S, Popadic D, Cvetkovic I, Mostarica-Stojkovic M. 2006. Strain difference in
810 susceptibility to experimental autoimmune encephalomyelitis between Albino Oxford and
811 Dark Agouti rats correlates with disparity in production of IL-17, but not nitric oxide. J
812 Neurosci Res 84:379–388.
813 Narcisse L, Scemes E, Zhao Y. 2005. The Cytokine IL-1 ᴺᴸ Transiently Enhances P2X 7
814 Receptor Expression and Function in Human Astrocytes. 258:245–258.
815 Nikolic L, Shen W, Nobili P, Virenque A, Ulmann L, Audinat E. 2018. Blocking TNFα-driven
816 astrocyte purinergic signaling restores normal synaptic activity in epilepsyBlocking TNFα-
817 driven astrocyte purinergic signaling restores normal synaptic activity in epilepsy. Glia in
818 Press:1–11.

819 Nimmerjahn A, Bergles DE. 2015. Large-scale recording of astrocyte activity. Curr Opin
820 Neurobiol [Internet] 32:95–106. Available from:
821 http://dx.doi.org/10.1016/j.conb.2015.01.015
822 Panatier A, Vallée J, Haber M, Murai KK, Lacaille JC, Robitaille R. 2011. Astrocytes are
823 endogenous regulators of basal transmission at central synapses. Cell 146:785–798.
824 Parpura V, Heneka MT, Montana V, Oliet SHR, Schousboe A, Haydon PG, Stout RF, Spray DC,
825 Reichenbach A, Pannicke T, Pekny M, Pekna M, Zorec R, Verkhratsky A. 2012. Glial cells
826 in (patho)physiology. J Neurochem [Internet] 121:4–27. Available from:
827 http://www.ncbi.nlm.nih.gov/pubmed/22251135
828 Porter JT, McCarthy KD. 1996. Hippocampal astrocytes in situ respond to glutamate released
829 from synaptic terminals. J Neurosci 16:5073–5081.
830 Prajeeth CK, Kronisch J, Khorooshi R, Knier B, Toft-Hansen H, Gudi V, Floess S, Huehn J,
831 Owens T, Korn T, Stangel M. 2017. Effectors of Th1 and Th17 cells act on astrocytes and
832 augment their neuroinflammatory properties. J Neuroinflammation 14:1–14.
833 Qian Y, Liu C, Hartupee J, Altuntas CZ, Gulen MF, Jane-Wit D, Xiao J, Lu Y, Giltiay N, Liu J,
834 Kordula T, Zhang QW, Vallance B, Swaidani S, Aronica M, Tuohy VK, Hamilton T, Li X.
835 2007. The adaptor Act1 is required for interleukin 17 - Dependent signaling associated with
836 autoimmune and inflammatory disease. Nat Immunol 8:247–256.
837 Rothhammer V, Quintana FJ. 2015. Control of autoimmune CNS inflammation by astrocytes.
838 Semin Immunopathol 37:625–638.
839 Schenk U, Westendorf AM, Radaelli E, Casati A, Ferro M, Fumagalli M, Verderio C, Buer J,
840 Scanziani E, Grassi F. 2008. Purinergic control of T cell activation by ATP released through
841 pannexin-1 hemichannels. Sci Signal 1:ra6.
842 Schläger C, Körner H, Krueger M, Vidoli S, Haberl M, Mielke D, Brylla E, Issekutz T, Cabanãs
843 C, Nelson PJ, Ziemssen T, Rohde V, Bechmann I, Lodygin D, Odoardi F, Flügel A. 2016.
844 Effector T-cell trafficking between the leptomeninges and the cerebrospinal fluid. Nature
845 [Internet] 530:349–353. Available from: http://dx.doi.org/10.1038/nature16939
846 Shen W, Nikolic L, Meunier C, Pfrieger F, Audinat E. 2017. An autocrine purinergic signaling
847 controls astrocyte-induced neuronal excitation. Sci Rep [Internet] 7:11280. Available from:
848 http://www.nature.com/articles/s41598-017-11793-x
849 Shigetomi E, Jackson-Weaver O, Huckstepp RT, O'Dell TJ, Khakh BS. 2013. TRPA1 Channels

Are Regulators of Astrocyte Basal Calcium Levels and Long-Term Potentiation via Constitutive D-Serine Release. J Neurosci 33:10143–10153.

Verkhratsky A, Parpura V, Vardjan N, Zorec R. 2019. Physiology of Astroglia. Adv Exp Med Biol 1175:45–91.

Voskuhl RR, Peterson RS, Song B, Ao Y, Morales LBJ, Tiwari-Woodruff S, Sofroniew M V. 2009. Reactive astrocytes form scar-like perivascular barriers to leukocytes during adaptive immune inflammation of the CNS. J Neurosci 29:11511–11522.

Wang X, Lou N, Xu Q, Tian G-F, Peng WG, Han X, Kang J, Takano T, Nedergaard M. 2006. Astrocytic Ca2+ signaling evoked by sensory stimulation in vivo. Nat Neurosci 9:816–823.

Yi W, Schlüter D, Wang X. 2019. Astrocytes in multiple sclerosis and experimental autoimmune encephalomyelitis: Star-shaped cells illuminating the darkness of CNS autoimmunity. Brain Behav Immun [Internet] 80:10–24. Available from: https://doi.org/10.1016/j.bbi.2019.05.029

Graphical Abstract

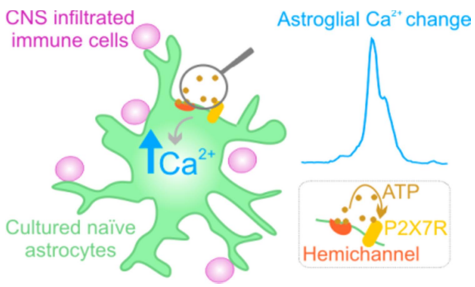

Application of the central nervous system (CNS) infiltrated immune cells induces a rapid increase in intracellular Ca^{2+} in cultured naïve astrocytes through glial purinergic receptor-mediated signaling. This provides an insight into the astroglial response to the immune cells in their local environment in CNS autoimmunity.

Figure legends

Figure 1.

CNS IIC application induces astroglial Ca^{2+} elevation.

(**a**) Upper: Cartoon of experimental approach for Ca^{2+} imaging of cultured naïve spinal cord astrocytes during bath application of CNS infiltrated immune cells (CNS IIC) isolated from the spinal cord of rat with EAE. Lower: First raw of images show purified cultured astrocytes immunostained for GFAP (green), Hoechst was used to stain the cell nuclei (blue), scale bar 50 µm; Bottom raw of images illustrate applied CNS IIC (yellow) in close proximity to astrocytes in the experimental set up, scale bar 20 µm. (**b**) Upper: Example traces of astroglial Ca^{2+} increases (Fluo-4 fluorescence) induced by the CNS IIC applied at concentrations of 5×10^3 cells/ml (left), 25×10^3 cells/ml (middle) and 50×10^3 cells/ml (right). Lower: Fractions of astrocytes responding to the applied CNS IIC. Graphs represent mean ± SD, number of responders out of total number of monitored astrocytes from 3 independent experiments is shown for each CNS IIC concentration applied, N = 3 EAE rats. (**c**) Summary graph comparing astrocyte Ca^{2+} changes from experiments shown in **b** (One-way ANOVA analysis on Ranks, Kruskal-Wallis test; $P < 0.001$; Dunn's post hoc test: $P = 0.036$ for 5×10^3 cells/ml versus 25×10^3 cells/ml, $P < 0.001$ for 25×10^3 cells/ml versus 50×10^3 cells/ml, $P < 0.001$ for 5×10^3 cells/ml versus 50×10^3/ml). n represent number of responders. (**d**) Time-lapse images of Fluo-4 fluorescence in astrocytes before (left) and during application of immune cells isolated from the cervical lymph node (Peripheral IC, middle) and from the CNS (CNS IIC, right) of EAE rat (each applied at 25×10^3 cells/ml concentration). Scale bar: 20 µm. (**e**) Left: Fractions of astrocytes responding to the Peripheral IC and CNS IIC. Graph represents mean ± SD, number of responders out of total number of monitored astrocytes from 4 independent experiments is shown, N = 4 EAE rats. Right: Green trace represents mean Ca^{2+} change in all responders (n = 32 astrocytes). Bottom: Ca^{2+} changes in individual astrocytes color-coded according to the fluorescence change. (**f**) Summary graph comparing astroglial Ca^{2+} changes from experiments shown in **e** (Wilcoxon Signed Rank Test; $z = 4.937$; $P < 0.001$). Data are shown as mean ± SD, n is number of responders. (**g**) Left: Schematic illustrating 2 consecutive applications of CNS IIC on astrocytes (CNS IIC concentration is 25×10^3 cells/ml). Right: Example traces from 12 astrocytes showing Ca^{2+} changes resulting from 1^{st} and 2^{nd} application of the CNS IIC. (**h**) Summary graph

comparing astroglial Ca^{2+} elevations induced by the 1st and 2nd application of the CNS IIC (Wilcoxon Signed Rank Test; n = 31 astrocytes from 3 independent experiments; $z = 1.470$; $P = 0.144$). Data are shown as mean ± SD. (**i**) Schematic illustrating measurement of astrocyte Ca^{2+} level in the presence of the CNS IIC or their matched conditioned medium (CNS IIC-conditioned medium). (**j**) Left: Images of Fluo-4 fluorescence in astrocytes during application of CNS IIC and CNS IIC-conditioned medium. Right: Fractions of responders. Graph represents mean ± SD, number of responders out of total number of monitored astrocytes from 5-6 independent experiments for each condition is shown, N = 4 EAE rats (Unpaired two-tailed Student's t test; t_9=5.413; $P < 0.001$). Scale bars: 20 µm. (**k**) Example traces and summary graph showing Ca^{2+} changes in astrocytes induced by the CNS IIC and by the CNS IIC-conditioned medium (Mann-Whitney test; $U = 159.000$; $P = 0.005$). n is number of responders. In box and whisker plots, central line shows the median, central dot shows the mean, the edges of the box define the upper and lower quartile values, and whiskers show the minimum-maximum range. Open circles represent independent experiments. Grey circles represent astrocytes. Grey rectangles depict immune cell application.

Figure 2.

CNS IIC-evoked Ca^{2+} increase in astrocytes persists in the presence of mGluR group I receptors and TRPA1 channels inhibitors.

(**a**) Schematic: Imaging of astroglial response to the CNS IIC application (25×10^3 cells/ml) in the control ECS and ECS containing blockers (100 µM CPCCOEt, 50 µM MPEP or 10 µM A967079). (**b**) Images of Fluo-4 fluorescence (left) and fractions of astrocytes (right) responding to the applied CNS IIC in interleaved Control and after the block of astroglial mGluR1 with CPCCOEt. Graph represents mean ± SD, number of responders out of total number of monitored astrocytes from 4 independent experiments for each condition is shown, N = 3 EAE rats (Unpaired two-tailed Student's t test; t_6=1.284; $P = 0.247$). Scale bars: 20 µm. (**c**) Example traces showing characteristics of astroglial Ca^{2+} changes induced by the CNS IIC in interleaved Control and in the presence of CPCCOEt. (**d**) Summary graph comparing CNS IIC-evoked Ca^{2+} changes in astrocytes from experiments shown in **b** (Unpaired two-tailed Student's t test; t_{102}=0.117; $P = 0.907$). n is number of responders. (**e**) Images of Fluo-4 fluorescence in astrocytes during application of the CNS IIC in interleaved Control and after the block of astroglial mGluR5 with

MPEP. Scale bars: 20 μm. (**f**) Fractions of astrocytes responding to the applied CNS IIC in interleaved Control and in the presence of MPEP. Graph represents mean ± SD, number of responders out of total number of monitored astrocytes from 5 independent experiments for each condition is shown, N = 3 EAE rats (Unpaired two-tailed Student's t test; t_8=1.403; P = 0.198). (**g, h**) Example traces (in **g**) and summary graph (in **h**) showing Ca^{2+} changes in astrocytes evoked by application of the CNS IIC in interleaved Control and with MPEP (in **h**: Mann-Whitney test; U = 1226.000; P = 0.266). n is number of responders. (**i**) Images of Fluo-4 fluorescence (left) and fractions of astrocytes (right) responding to the CNS IIC application in interleaved Control and after the astroglial TRPA1 channels block with A967079. Graph represents mean ± SD, number of responders out of total number of monitored astrocytes from 4 independent experiments for each condition is shown, N = 4 EAE rats (Mann-Whitney test; U = 7.500; P = 0.886). Scale bars: 20 μm. (**j**) Example traces of Ca^{2+} changes in astrocytes induced by the CNS IIC in interleaved Control and in the presence of A967079. (**k**) Summary graph comparing astroglial Ca^{2+} elevations from experiments in **i** (Mann-Whitney test, U = 665.000; P = 0.477). n is number of responders. Box and whisker plots as defined in **Figure 1**. Open circles represent independent experiments. Grey rectangles depict immune cell application.

Figure 3.

P2X7 receptor-mediated signaling is required for CNS IIC-induced Ca^{2+} increase in astrocytes.

(**a**) Schematic: Imaging of astrocyte Ca^{2+} level during application of CNS IIC (25×10^3 cells/ml) in the control ECS and ECS containing the blockers of astroglial purinergic receptors (50 μM PPADS, 10 μM MRS2179 receptors or 10 μM A438079). (**b**) CNS IIC-induced Ca^{2+} changes in individual astrocytes color-coded according to the fluorescence change from interleaved Control and after application of PPADS. Bottom: Fractions of responders. Graph represents mean ± SD, number of responders out of total number of monitored astrocytes from 4-5 independent experiments for each condition is shown, N = 3 EAE rats (Unpaired two-tailed Student's t test; t_7=5.447; $P < 0.001$). (**c**) Example traces showing characteristics of Ca^{2+} elevations in astrocytes evoked by the CNS IIC from interleaved Control and after the block of P2 receptors with PPADS. (**d**) Summary graph comparing CNS IIC-evoked Ca^{2+} changes in astrocytes from experiments shown in **b** (Mann-Whitney test, U = 70.000; $P < 0.001$). n is number of responders.

(**e**) CNS IIC-induced Ca^{2+} changes in individual astrocytes color-coded according to the fluorescence change from interleaved Control and after application of MRS2179. Bottom: Fractions of responders. Graph represents mean ± SD, number of responders out of total number of monitored astrocytes from 3 independent experiments for each condition is shown, N = 3 EAE rats (Unpaired two-tailed Student's t test; t_4=0.133; P = 0.901). (**f**) Example traces displaying Ca^{2+} changes in astrocytes evoked by the CNS IIC from interleaved Control and after the block of P2Y1 receptors with MRS2179. (**g**) Summary graph comparing astroglial Ca^{2+} changes from experiments shown in **e** (Mann-Whitney test, U = 366.000; P = 0.418). n is number of responders. (**h**) Left: CNS IIC-induced Ca^{2+} changes in individual astrocytes color-coded according to the fluorescence change from interleaved Control and after application of A438079. Right: Fraction of responders. Graph represents mean ± SD, number of responders out of total number of monitored astrocytes from 3 independent experiments for each condition is shown, N = 3 EAE rats (Unpaired two-tailed Student's t test; t_4=7.228; P = 0.002). (**i**) Example traces displaying Ca^{2+} elevations in astrocytes evoked by the CNS IIC from interleaved Control and after application of A438079 to block P2X7 receptors. (**j**) Summary plot comparing astrocyte Ca^{2+} changes from experiments shown in **h** (Mann-Whitney test, U = 10.000; P < 0.001). n is number of responders. (**k**) Example trace showing astroglial Ca^{2+} increase evoked by application of BzATP (depicted with blue rectangle) to activate astroglial P2X7 receptors. (**l**) Graph comparing astrocyte Ca^{2+} changes induced by BzATP and CNS IIC in interleaved experiments (Mann-Whitney test, U = 562.000; P = 0.541), 3 EAE rats, n is number of astrocytes from 3 independent experiments for each condition. Box and whisker plots as defined in **Figure 1**. Open circles represent independent experiments. Grey rectangles depict immune cell application.

Figure 4.

CNS IIC-induced P2X7 receptor activation and Ca^{2+} increase in astrocytes depend on astroglial hemichannels.

(**a**) Schematic of experimental approach for quantitative measurement of ATP from CNS IIC and Peripheral IC using Luciferin-luciferase bioluminescence assay. Right: Graph comparing ATP release from CNS IIC and Peripheral IC (Unpaired two-tailed Student's t test; N = 8 EAE rats; 8 measurements for each immune cell group; t_{14} = 0.582; P = 0.570). (**b**) Schematic: Imaging of astrocyte Ca^{2+} level during application of the CNS IIC in control ECS and with brefeldin A (2

µg/mL Bref. A) or carbenoxolone (50 µM CBX) to disrupt ATP release from astrocytes. (**c**) Left: Images of Fluo-4 fluorescence in astrocytes during application of the CNS IIC in interleaved Control and after treatment with Bref. A. Scale bars: 20 µm. Right: Fractions of responders. Graph represents mean ± SD, number of responders out of total number of monitored astrocytes from 3-4 independent experiments for each condition is shown, N = 3 EAE rats (Unpaired two-tailed Student's t test; t_5=0.924; P = 0.398). (**d**) Example traces of Ca^{2+} elevations in astrocytes induced by the CNS IIC in interleaved Control and in Bref. A. (**e**) Summary graph comparing CNS IIC-evoked Ca^{2+} changes in astrocytes from experiments shown in **c** (Mann-Whitney test, U = 507.000; P = 0.510). n is number of responders. (**f**) Left: Images of Fluo-4 fluorescence in astrocytes during application of the CNS IIC from interleaved Control and with CBX. Scale bars: 20 µm. Right: Fractions of responders. Graph represents mean ± SD, number of responders out of total number of monitored astrocytes from 3-4 independent experiments for each condition is shown, N = 3 EAE rats (Unpaired two-tailed Student's t test; t_5=3.858; P = 0.012). (**g**) Example traces showing Ca^{2+} changes in astrocytes induced by the CNS IIC in interleaved Control and with CBX. (**h**) Summary plot comparing CNS IIC-evoked Ca^{2+} changes in astrocytes from experiments shown in **f** (Mann-Whitney test, U = 47.000; P = 0.004). n is number of responders. (**i**) Example traces from 5 astrocytes showing characteristics of Ca^{2+} changes evoked by the CNS IIC and ATP (depicted by blue rectangle) with CBX present. CNS IIC are applied at 25 × 10^3 cells/ml concentration. Box and whisker plots as defined in **Figure 1**. Open circles represent independent experiments. Grey rectangles depict immune cell application.

Figure 5.

CNS infiltrated $CD4^+$ T cells specifically increase astroglial Ca^{2+} and interact with astrocytes during EAE.

(**a**) Time-lapse images of Fluo-4 fluorescence in astrocytes before (left) and during application of $CD4^+$ CNS infiltrated T cells ($CD4^+$ CNS ITC, middle) and the rest of the CNS infiltrated immune cell population (CNS IIC without $CD4^+$ ITC, right) isolated from the spinal cord of EAE rat (each applied at 25 × 10^3 cells/ml concentration). Scale bar: 50 µm. (**b**) Left: Fractions of astrocytes responding to the applied $CD4^+$ CNS ITC and CNS IIC without $CD4^+$ ITC. Graph represents mean ± SD, number of responders out of total number of monitored astrocytes from 3 experiments is shown, N = 3 EAE rats (Paired two-tailed Student's t test; t_2=6.608; P = 0.022).

Right: Green trace shows a mean Ca^{2+} change in all responders to the $CD4^+$ CNS ITC and to the subsequently applied CNS IIC without $CD4^+$ ITC (n = 36 astrocytes). Bottom: Ca^{2+} changes in individual astrocytes color-coded according to the fluorescence change. (**c**) Summary graph comparing astrocyte Ca^{2+} levels after application of the $CD4^+$ CNS ITC and CNS IIC without $CD4^+$ ITC (Wilcoxon Signed Rank Test; $z = 5.232$; $P < 0.001$) and after application of the CNS IIC in the interleaved experiments (Mann-Whitney test, $U = 495.000$; $P = 0.323$). Data are shown as mean ± SD, n represent number of responders. (**d, e**) Confocal z-projection (in **d**) and orthogonal view (in **e**) images of CD4 labeled T cells (magenta) and GFAP labeled astrocytes (green) from grey (in red rectangle) and white (in blue rectangle) matter of the EAE rat spinal cord. Images are maximum intensity projections of 6.3 µm z-stack. Scale bars: 10 µm. Average fraction of $CD4^+$ infiltrated T cells interacting with GFAP labeled astrocytes in the spinal cord of EAE rat (white and grey matter) is shown in **e** (bottom). Graph represents mean ± SD; N = 3 EAE rats, 3-4 spinal cord sections per animal were analyzed (depicted with squares). Box and whisker plots as defined in **Figure 1**. Open circles represent independent experiments. Grey rectangles depict immune cell application. Grey circles represent astrocytes.

Figure S1: Assessment of culture purity (Related to Figure 1).

Confocal images show cultured cells immunostained for astrocyte-specific marker (anti-GFAP, GFAP, green), microglia-specific marker (anti-Iba1, Iba1, magenta), and oligodendrocyte-specific marker (anti-CNPase, CNPase, grey). Cell Nuclei were stained with DAPI (blue). Graph shows % of $GFAP^+$, $Iba1^+$ and $CNPase^+$ cells (485 nuclei were analyzed from 6 coverslips). $GFAP^+$ astrocytes constitute more than 90% of cultured cells (447 out of 485 cells), while the remaining cells represent $Iba1^+$ microglia (23 out of 485 cells). $CNPase^+$ oligodendrocytes were not detected (0/485 cells). In box and whisker plots, central line shows the median, central dot shows the mean, the edges of the box define the upper and lower quartile values, and whiskers show the minimum-maximum range. Scale bar: 20 µm.

Figure S2: Ca^{2+} responses of astrocytes induced by the CNS IIC isolated from female and male rats with EAE (related to Figure 1).

(a) Fractions of astrocytes responding with a Ca^{2+} increase to the applied CNS IIC isolated from the female (N = 8 EAE rats) and male (N = 6 EAE rats) rats with EAE. Graph represents mean ±

SD, number of responders out of total number of monitored astrocytes from 8-10 experiments is shown (Unpaired two-tailed Student's t test; t_{16}=0.721; P = 0.481). Open circles represent independent experiments. **(b)** Graph comparing astroglial Ca^{2+} changes induced by the CNS IIC of female and male EAE rats (Mann-Whitney test; U = 4253.000; P = 0.977). n is number of responders. CNS IIC are applied at 25 × 10^3 cells/ml concentration. In box and whisker plots, central line shows the median, central dot shows the mean, the edges of the box define the upper and lower quartile values, and whiskers show the minimum-maximum range.

Figure S3: Immunohistochemistry of the spinal cord of rat with EAE (related to Figure 5). Confocal images show maximum z-projection of EAE rat spinal cord immunostained for $CD4^+$ T cells (anti-CD4, CD4, magenta) and surrounding astrocytes (anti-GFAP, GFAP, green). Infiltrated $CD4^+$ T cells are spread in the parenchyma and surrounded by astrocytes. Scale bar: 20 μm. Graph shows density of CNS infiltrated $CD4^+$ T cells in the spinal cord of EAE rat (N = 3 EAE rats). Data are shown as mean ± SD. 3-4 spinal cord sections per animal were analyzed (depicted with squares).

Figure 1.

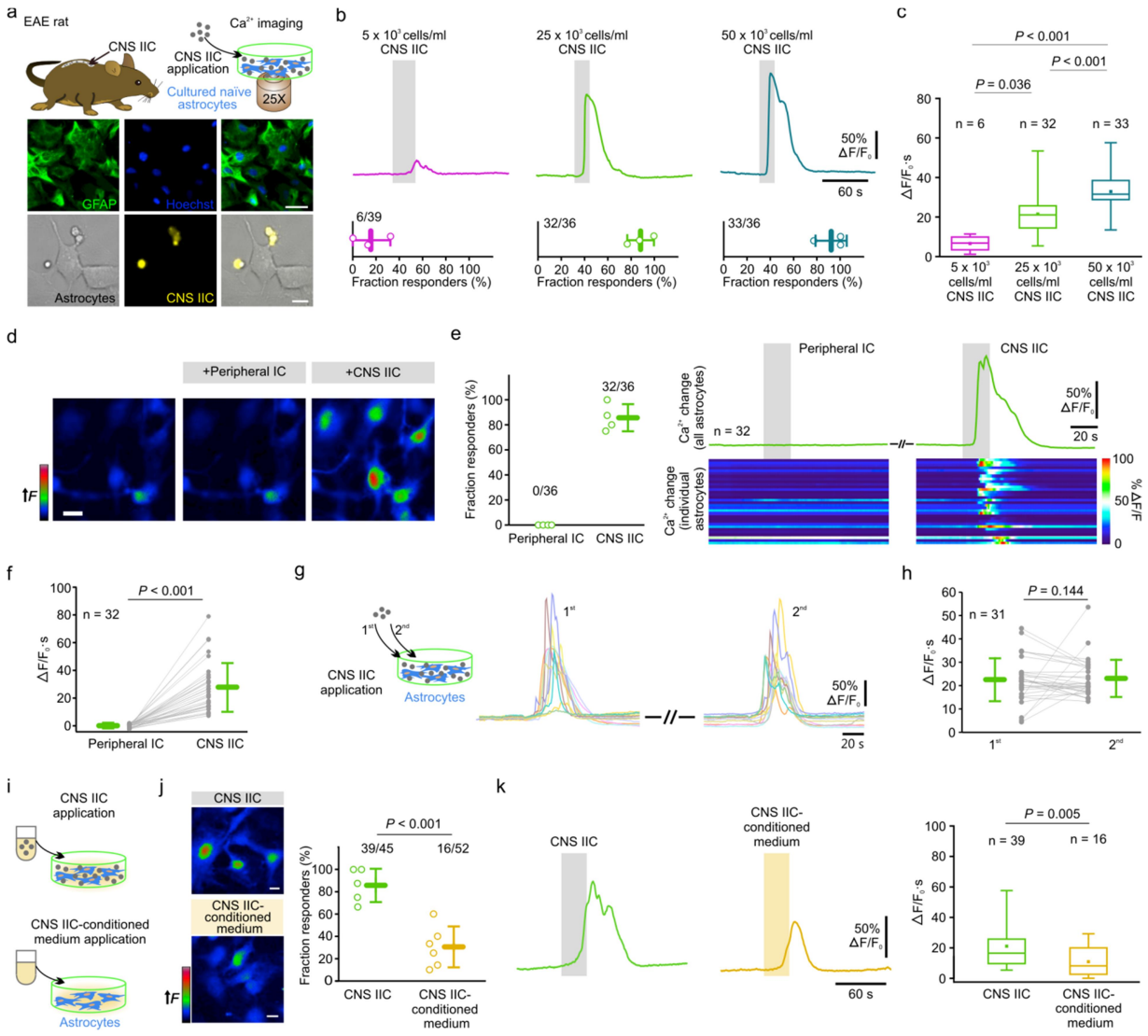
a
EAE rat
CNS IIC
Ca2+ imaging
CNS IIC application
Cultured naïve astrocytes
25X
GFAP
Hoechst
Astrocytes
CNS IIC
b
5 x 10³ cells/ml CNS IIC
25 x 10³ cells/ml CNS IIC
50 x 10³ cells/ml CNS IIC
50% ΔF/F0
60 s
6/39
32/36
33/36
0 20 40 60 80 100
Fraction responders (%)
c
P < 0.001
P < 0.001
P = 0.036
n = 6
n = 32
n = 33
ΔF/F0·s
5 x 10³ cells/ml CNS IIC
25 x 10³ cells/ml CNS IIC
50 x 10³ cells/ml CNS IIC
d
+Peripheral IC
+CNS IIC
↑F
e
Fraction responders (%)
32/36
0/36
Peripheral IC
CNS IIC
Peripheral IC
CNS IIC
Ca2+ change (all astrocytes)
n = 32
50% ΔF/F0
20 s
Ca2+ change (individual astrocytes)
100
50
0
% ΔF/F
f
P < 0.001
n = 32
ΔF/F0·s
Peripheral IC
CNS IIC
g
1st
2nd
CNS IIC application
Astrocytes
50% ΔF/F0
20 s
h
P = 0.144
n = 31
ΔF/F0·s
1st
2nd
i
CNS IIC application
CNS IIC-conditioned medium application
Astrocytes
j
CNS IIC
CNS IIC-conditioned medium
↑F
P < 0.001
39/45
16/52
Fraction responders (%)
CNS IIC
CNS IIC-conditioned medium
k
CNS IIC
CNS IIC-conditioned medium
50% ΔF/F0
60 s
P = 0.005
n = 39
n = 16
ΔF/F0·s
CNS IIC
CNS IIC-conditioned medium

Figure 2.

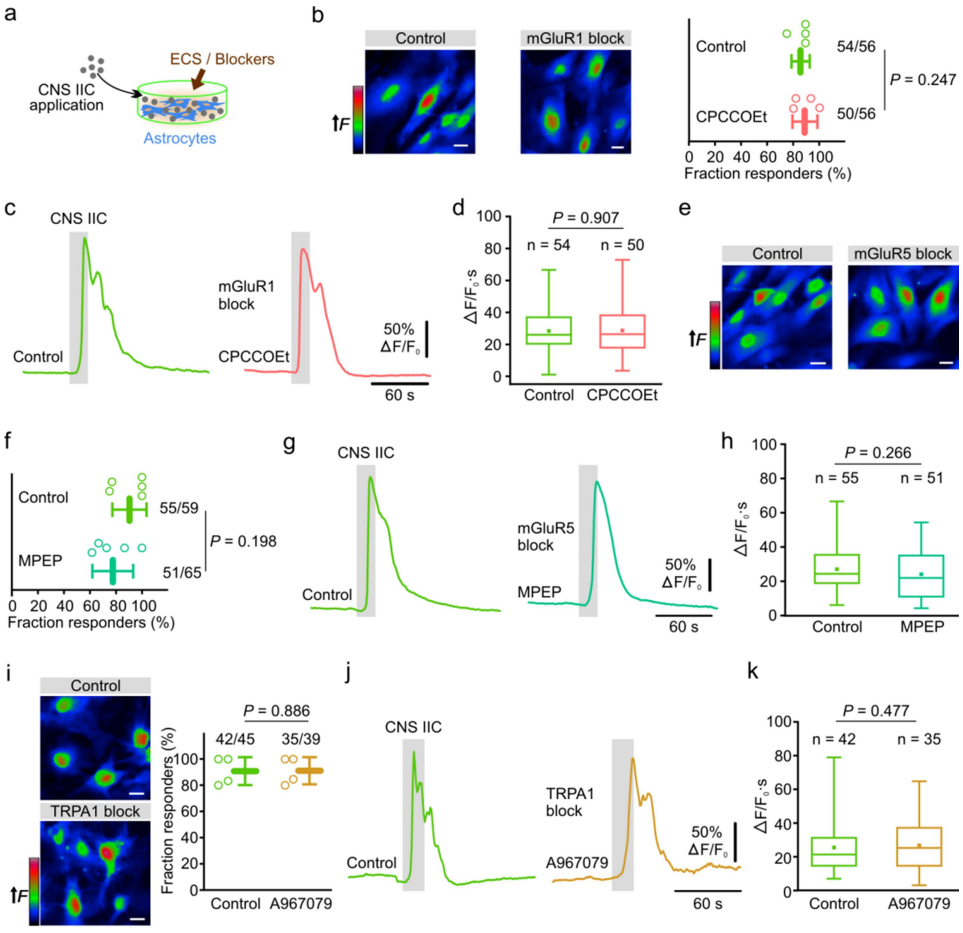
a
ECS / Blockers
CNS IIC application
Astrocytes
b
Control
mGluR1 block
Control
54/56
CPCCOEt
50/56
P = 0.247
0 20 40 60 80 100
Fraction responders (%)
c
CNS IIC
mGluR1 block
Control
CPCCOEt
50% ΔF/F0
60 s
d
P = 0.907
n = 54
n = 50
ΔF/F0*s
Control
CPCCOEt
e
Control
mGluR5 block
f
Control
55/59
MPEP
51/65
P = 0.198
0 20 40 60 80 100
Fraction responders (%)
g
CNS IIC
mGluR5 block
Control
MPEP
50% ΔF/F0
60 s
h
P = 0.266
n = 55
n = 51
ΔF/F0*s
Control
MPEP
i
Control
TRPA1 block
P = 0.886
42/45
35/39
Fraction responders (%)
Control
A967079
j
CNS IIC
TRPA1 block
Control
A967079
50% ΔF/F0
60 s
k
P = 0.477
n = 42
n = 35
ΔF/F0*s
Control
A967079

Figure 3.

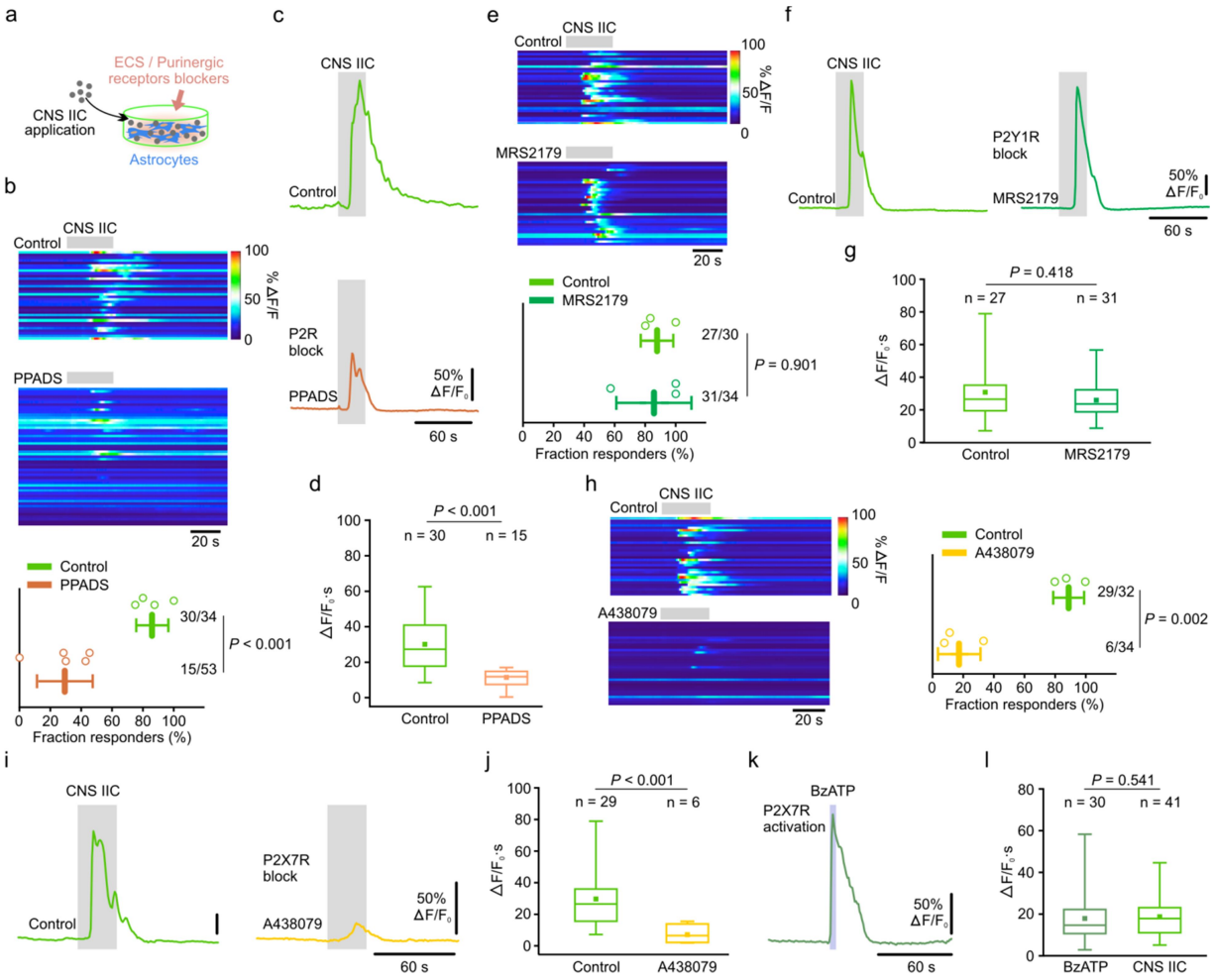
a
ECS / Purinergic receptors blockers
CNS IIC application
Astrocytes
b
CNS IIC
Control
100
50
0
% ΔF/F
PPADS
20 s
Control
PPADS
30/34
15/53
P < 0.001
0 20 40 60 80 100
Fraction responders (%)
c
CNS IIC
Control
P2R block
PPADS
50% ΔF/F0
60 s
d
P < 0.001
n = 30
n = 15
ΔF/F0·s
Control
PPADS
e
CNS IIC
Control
MRS2179
20 s
Control
MRS2179
27/30
31/34
P = 0.901
0 20 40 60 80 100
Fraction responders (%)
f
CNS IIC
Control
P2Y1R block
MRS2179
50% ΔF/F0
60 s
g
P = 0.418
n = 27
n = 31
ΔF/F0·s
Control
MRS2179
h
CNS IIC
Control
A438079
20 s
Control
A438079
29/32
6/34
P = 0.002
0 20 40 60 80 100
Fraction responders (%)
i
CNS IIC
Control
P2X7R block
A438079
50% ΔF/F0
60 s
j
P < 0.001
n = 29
n = 6
ΔF/F0·s
Control
A438079
k
BzATP
P2X7R activation
50% ΔF/F0
60 s
l
P = 0.541
n = 30
n = 41
ΔF/F0·s
BzATP
CNS IIC

Figure 4.

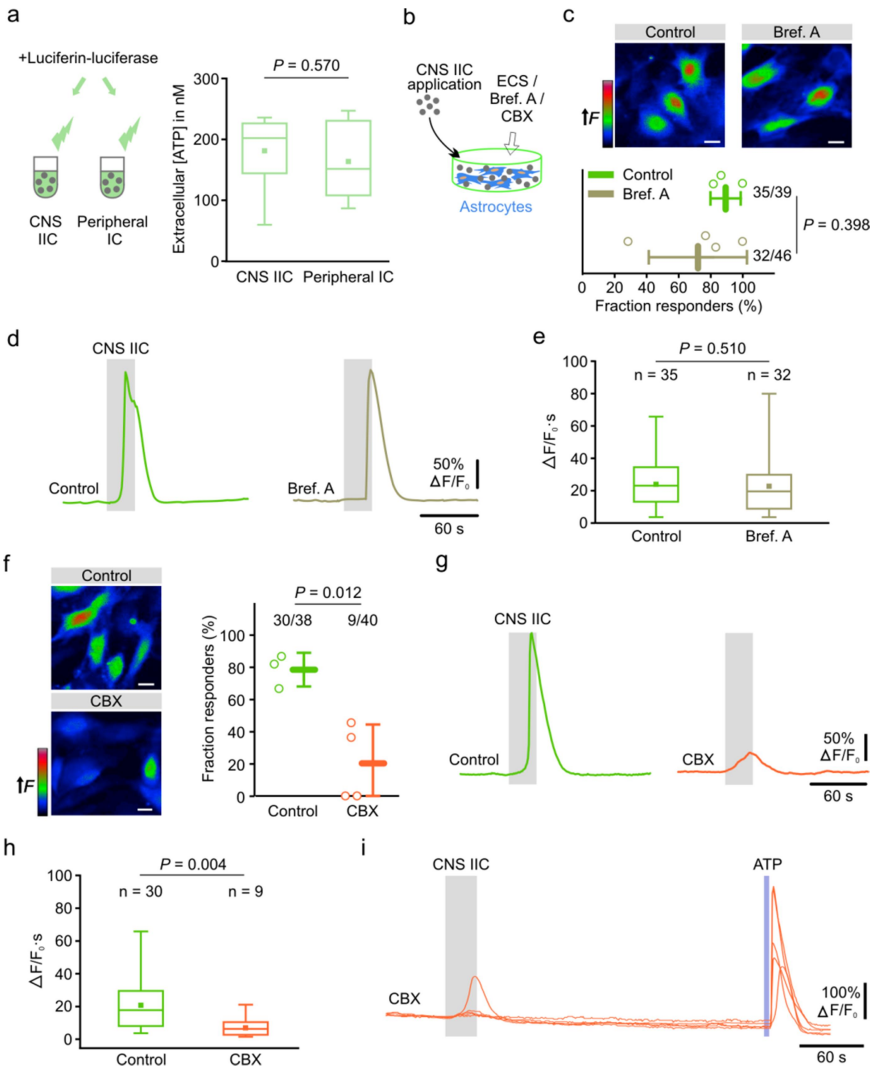
a
+Luciferin-luciferase
CNS IIC
Peripheral IC
Extracellular [ATP] in nM
300
200
100
0
P = 0.570
CNS IIC
Peripheral IC
b
CNS IIC application
ECS / Bref. A / CBX
Astrocytes
c
Control
Bref. A
↑F
Control
Bref. A
35/39
32/46
P = 0.398
0 20 40 60 80 100
Fraction responders (%)
d
CNS IIC
Control
Bref. A
50% ΔF/F0
60 s
e
P = 0.510
n = 35
n = 32
ΔF/F0·s
100
80
60
40
20
0
Control
Bref. A
f
Control
CBX
↑F
P = 0.012
30/38
9/40
Fraction responders (%)
100
80
60
40
20
0
Control
CBX
g
CNS IIC
Control
CBX
50% ΔF/F0
60 s
h
P = 0.004
n = 30
n = 9
ΔF/F0·s
100
80
60
40
20
0
Control
CBX
i
CNS IIC
ATP
CBX
100% ΔF/F0
60 s

Figure 5.

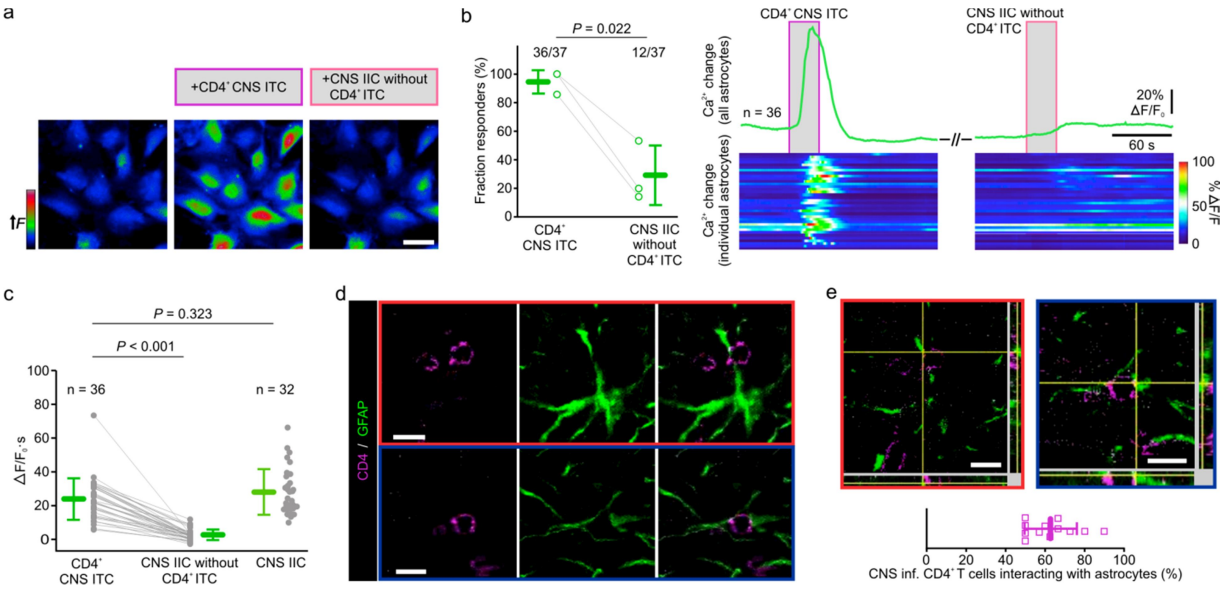
a
+CD4⁺ CNS ITC
+CNS IIC without CD4⁺ ITC
tF
b
P = 0.022
36/37
12/37
Fraction responders (%)
CD4⁺ CNS ITC
CNS IIC without CD4⁺ ITC
CD4⁺ CNS ITC
CNS IIC without CD4⁺ ITC
Ca²⁺ change (all astrocytes)
n = 36
20% ΔF/F₀
60 s
Ca²⁺ change (individual astrocytes)
100
50
0
% ΔF/F
c
P = 0.323
P < 0.001
n = 36
n = 32
ΔF/F₀ s
CD4⁺ CNS ITC
CNS IIC without CD4⁺ ITC
CNS IIC
d
CD4 / GFAP
e
CNS inf. CD4⁺ T cells interacting with astrocytes (%)

Figure S1.

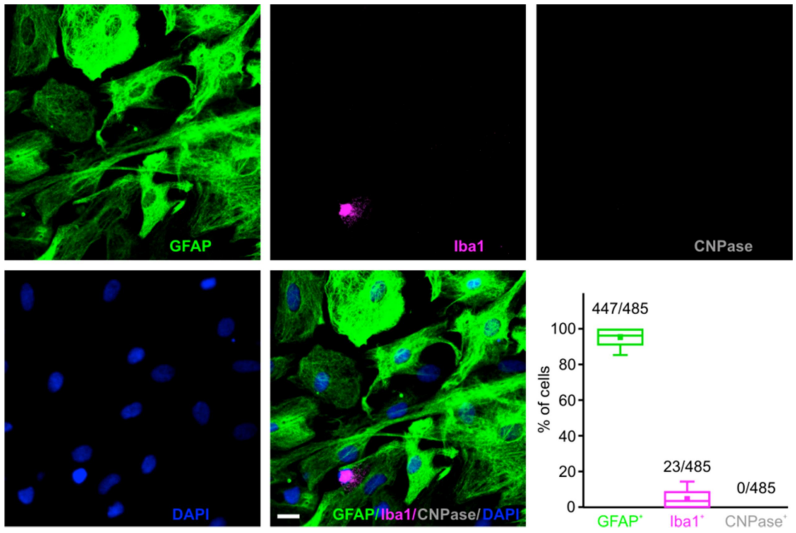

Figure S2.

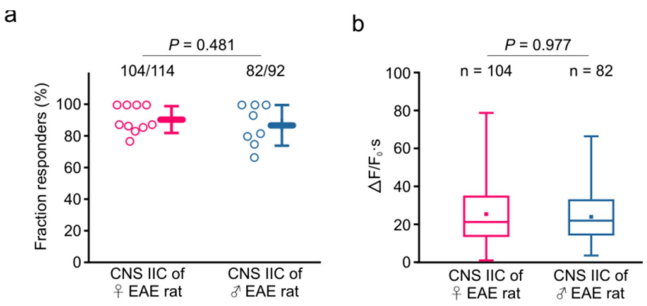

Figure S3.

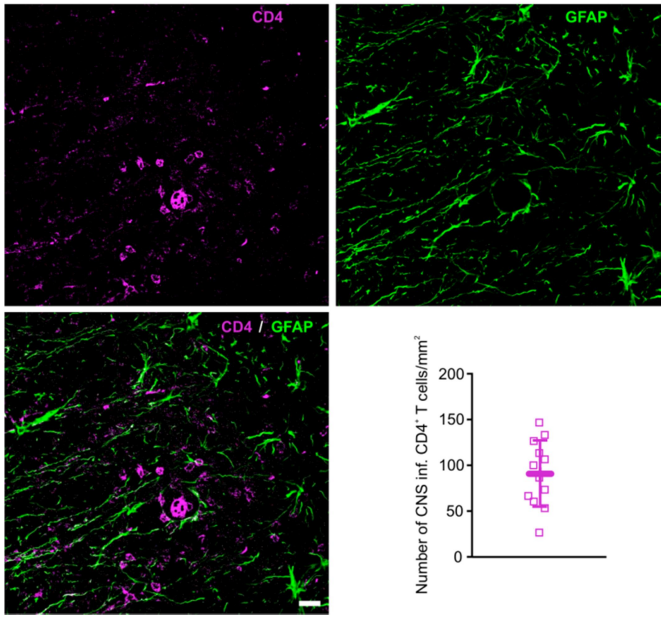
CD4
GFAP
CD4 / GFAP
Number of CNS inf. CD4+ T cells/mm2
200
150
100
50
0